Water storage redistribution over East China, between 2003 and 2015, driven by intra- and inter-annual climate variability

He, Q., Chun, K. P., Fok, H. S., Chen, Q., Dieppois, B. & Massei, N.

Original citation & hyperlink:
He, Q, Chun, KP, Fok, HS, Chen, Q, Dieppois, B & Massei, N 2020, 'Water storage redistribution over East China, between 2003 and 2015, driven by intra- and inter-annual climate variability', Journal of Hydrology, vol. 583, 124475.
https://dx.doi.org/10.1016/j.jhydrol.2019.124475

DOI 10.1016/j.jhydrol.2019.124475
ISSN 0022-1694

Publisher: Elsevier

Elsevier Editorial System(tm) for Journal of Hydrology or its open access mirror
Manuscript Draft

Manuscript Number: HYDROL32401R2

Title: Water storage redistribution over East China, between 2003 and 2015, driven by intra- and inter-annual climate variability

Article Type: Research paper

Keywords: Terrestrial water storage; Asian monsoons; El Nino Southern Oscillations; East China; climate variability

Corresponding Author: Dr. Kwok Pan Chun,

Corresponding Author's Institution: Hong Kong Baptist University

First Author: Qing He

Order of Authors: Qing He; Kwok Pan Chun; Hok Sum Fok; Qiang Chen; Bastien Dieppois; Nicolas Massei

Abstract: Abstract
National development and resilience are strained by shifting regional water storage patterns. The water shifting pattern has been found over China, but the underlying climate mechanisms of the pattern remain largely unexplored. In this study, how shifting regional moisture conditions are related to intra-annual and inter-annual atmospheric oscillations can be explored by terrestrial water storage (TWS) derived from the Gravity Recovery and Climate Experiment (GRACE). Using a principal component analysis (PCA), the TWSs over the East China were divided into two spatial empirical orthogonal functions (EOFs), accounting for more than 70% of the total spatial variance. The first TWS EOF is related to the seasonal variation, whereas the second TWS EOF is associated with the spatial distribution of TWS trend. In addition, the PCA trend results for precipitation and actual evapotranspiration (ET) are consistent with TWS, with a correlation of 0.44 ($p << 0.05$) and -0.47 ($p << 0.05$), respectively. Based on these PCA results, the Yangtze River Basin (YARB) was wetting, while the North China Plain (NCP) was drying between 2003 and 2015. This unbalance water distribution pattern was potentially linked to regional changes of the Hadley-type meridional circulation which aggravated the unevenness between north and south water distributions over the East China. Furthermore, a wavelet transform coherence (WTC) analysis was used for investigating multi-scale relationships between TWS and different climate factors. The local wind intensity and Asian monsoons were related to the regional unbalance TWS pattern on an intra-annual scale, with significance correlations of -0.49 ($p << 0.05$) and 0.9 ($p << 0.05$) respectively. Meanwhile El Nino Southern Oscillations (ENSO) was significantly negatively linked (correlation of -0.41, $p << 0.05$) with TWS variability at the inter-annual scale. However, based on partial WTC results, the association between ENSO and TWS can be explained away by the Asian monsoons, so that ENSO is only indirectly related to TWS through monsoons. Overall, the approaches and results of this study not only explained that the shifting TWS distribution over the East China was related to varying strength of local wind intensity and Asian monsoons, and ENSO at intra-annual and

inter-annual scales respectively, but also provided a framework for studying TWS redistribution over other regions, which are crucial for sustainable regional development and resilient water future.

Abstract

National development and resilience are strained by shifting regional water storage patterns. The water shifting pattern has been found over China, but the underlying climate mechanisms of the pattern remain largely unexplored. In this study, how shifting regional moisture conditions are related to intra-annual and inter-annual atmospheric oscillations can be explored by terrestrial water storage (TWS) derived from the Gravity Recovery and Climate Experiment (GRACE). Using a principal component analysis (PCA), the TWSs over the East China were divided into two spatial empirical orthogonal functions (EOFs), accounting for more than 70% of the total spatial variance. The first TWS EOF is related to the seasonal variation, whereas the second TWS EOF is associated with the spatial distribution of TWS trend. In addition, the PCA trend results for precipitation and actual evapotranspiration (ET) are consistent with TWS, with a correlation of 0.44 ($p << 0.05$) and -0.47 ($p << 0.05$), respectively. Based on these PCA results, the Yangtze River Basin (YARB) was wetting, while the North China Plain (NCP) was drying between 2003 and 2015. This unbalance water distribution pattern was potentially linked to regional changes of the Hadley-type meridional circulation which aggravated the unevenness between north and south water distributions over the East China. Furthermore, a wavelet transform coherence (WTC) analysis was used for investigating multi-scale relationships between TWS and different climate factors. The local wind intensity and Asian monsoons were related to the regional unbalance TWS pattern on an intra-annual scale, with significance correlations of -0.49 ($p << 0.05$) and 0.9 ($p << 0.05$) respectively. Meanwhile El Nino Southern Oscillations (ENSO) was significantly negatively linked (correlation of -0.41, $p << 0.05$) with TWS variability at the inter-annual scale. However, based on partial WTC results, the association between ENSO and TWS can be explained away by the Asian monsoons, so that ENSO is only indirectly related to TWS through monsoons. Overall, the approaches and results of this study not only explained that the shifting TWS distribution over the East China was related to varying strength of local wind intensity and Asian monsoons, and ENSO at intra-annual and inter-annual scales respectively, but also provided a framework for studying TWS redistribution over other regions, which are crucial for sustainable regional development and resilient water future.

***Highlights (3 to 5 bullet points (maximum 85 characters including spaces per bullet point)**

Highlights

- Unbalance water distribution over the East China was found during 2003-2015.
- Asian monsoons positively contributed to unbalance pattern at intra-annual scale.
- ENSO negatively contributed to unbalance pattern at inter-annual scale.

Water storage redistribution over East China, between 2003 and 2015, driven by intra- and inter-annual climate variability

Qing He[1], Kwok Pan Chun[1]*, Hok Sum Fok[2], Qiang Chen[3], Bastien Dieppois[4], Nicolas Massei[5],

[1] Department of Geography, Hong Kong Baptist University, Hong Kong, China

[2] School of Geodesy and Geomatics, Wuhan University, Wuhan 430079, China

[3] Geophysics Laboratory, Faculty of Science, Technology and Communication, University of Luxembourg, 6, Avenue de la Fonte, L-4364 Esch-sur-Alzette, Luxembourg

[4] Coventry University, UK

[5] The University of Rouen Normandy, France

***** Corresponding author:

Kowk Pan Chun, Department of Geography, Hong Kong Baptist University, Kowloon Tong, Hong Kong, China. E-mail: kpchun@hkbu.edu.hk

Highlights

- Unbalance water distribution over the East China was found during 2003-2015.
- Asian monsoons positively contributed to unbalance pattern at intra-annual scale.
- ENSO negatively contributed to unbalance pattern at inter-annual scale.

Abstract

National development and resilience are strained by shifting regional water storage patterns. The water shifting pattern has been found over China, but the underlying climate mechanisms of the pattern remain largely unexplored. In this study, how shifting regional moisture conditions are related to intra-annual and inter-annual atmospheric oscillations can be explored by terrestrial water storage (TWS) derived from the Gravity Recovery and Climate Experiment (GRACE). Using a principal component analysis (PCA), the TWSs over the East China were divided into two spatial empirical orthogonal functions (EOFs), accounting for more than 70% of the total spatial variance. The first TWS EOF is related to the seasonal variation, whereas the second TWS EOF is associated with the spatial distribution of TWS trend. In addition, the PCA trend results for precipitation and actual evapotranspiration (ET) are consistent with TWS, with a correlation of 0.44 ($p << 0.05$) and -0.47 ($p << 0.05$), respectively. Based on these PCA results, the Yangtze River Basin (YARB) was wetting, while the North China Plain (NCP) was drying between 2003 and 2015. This unbalance water distribution pattern was potentially linked to regional changes of the Hadley-type meridional circulation which aggravated the unevenness between north and south water distributions over the East China. Furthermore, a wavelet transform coherence (WTC) analysis was used for investigating multi-scale relationships between TWS and different climate factors. The local wind intensity and Asian monsoons were related to the regional unbalance TWS pattern on an intra-annual scale, with significance correlations of -0.49 (at $p << 0.05$) and 0.9 (at $p << 0.05$) respectively. Meanwhile El Nino Southern Oscillations (ENSO) was significantly negatively linked (correlation of -0.41, $p << 0.05$) with TWS variability at the inter-annual scale. However, based on partial WTC results, the association between ENSO and TWS can be explained away by the Asian monsoons, so that ENSO is only indirectly related to TWS through monsoons. Overall, the approaches and results of this study not only explained that the shifting TWS distribution over the East China was related to varying strength of local wind intensity and Asian monsoons, and ENSO at intra-annual and inter-annual scales respectively, but also provided a framework for studying TWS redistribution over other regions, which are crucial for sustainable regional development and resilient water future.

Key Words:

Terrestrial water storage; Asian monsoons; El Nino Southern Oscillations; East China; climate variability

1. Introduction

Regional water redistributions emerged from changing global climate at various spatiotemporal scales (Näschen et al., 2019), and these redistributions caused hydrological hazards and uneven water resources (Sharma and Shakya, 2006). Water challenges over China are related to a shifting North and South gradient due to irregular seasonality (Cheng et al., 2009). A large coastal region over the East China has a continental monsoon climate with wet summers and dry winters (Domrös and Gongbing, 1988). Spatially, annual precipitation in China varies from less than 50 mm.year^{-1} in the northwest region, to more than 1600 mm.year^{-1} in the southeast region (Cheng et al., 2009). This uneven north to south precipitation distribution has been observed from the late 1970s (Ding et al., 2009; Wang, 2001; Yang and Lau, 2004). Different explanations of potential drivers were suggested, including a weakening of the Asian summer monsoon (Wang, 2001), variations of sea surface temperature (SST) in the Pacific, Indian and Atlantic Oceans (Wang and An, 2002; Yang and Lau, 2004), and changes in snow coverage over Tibetan Plateau (Ding et al., 2009).

Changing catchment storage has been a derivative quantity from a water balance equation (Peixoto and Oort, 1992). The Gravity Recovery and Climate Experiment (GRACE) provided time-variable terrestrial water storage (TWS) measurements based on remote sensing (Xie et al., 2018; Zhao et al., 2015). Hydrological signals over world major river basins were well reconstructed from the GRACE data (Schmidt et al., 2006). For example, Reager and Famiglietti (2009) designed a monthly flood index based on the global water storage distribution from GRACE. The accuracy of global TWS estimated from GRACE had been further evaluated in Landerer and Swenson (2012).

Focusing on China, GRACE has been used to quantify TWS variations, estimate runoff and monitor hydrological extremes (Li et al., 2016; Luo et al., 2016; Zhang et al., 2016; Zhao et al., 2015). Over China, the TWS trend showed uneven spatial pattern: decreasing in North China, while increasing in the western and southern China (Zhao et al., 2015). For specific regions, TWS studies can be found for the North China Plain (NCP) region (Su et al., 2011), the Yellow River Basin (Li et al., 2016), the Pearl River Basin (Luo et al., 2016), the Yangtze River Basin (YARB) (Fok and He, 2018; Zhang et al., 2016), southwestern China (Tang et al., 2014). However, there are rarely studies focusing the spatiotemporal TWS dynamic over the East China, the most developed region in China (Démurger et al., 2002).

The variability of TWS over China has been attributed to the monsoons and teleconnections such as El Nino Southern Oscillation (ENSO) (Long et al., 2014; Ni et al., 2018; Tang et al., 2014; Zhang et al., 2015). ENSO has been demonstrated to have significant impacts on precipitation and TWS over China (Han et al., 2019; Luo et al., 2016; Sun et al., 2017; Yang et al., 2018; Zhang et al., 2015). Although abovementioned studies discussed the possible roles of monsoons and ENSO to the spatiotemporal patterns of TWS in China, how TWS is related to ENSO and monsoons simultaneously at different spatial and temporal scales have not been widely studied. In this study, the Principle Component Analysis (PCA), Wavelet Transform Coherence (WTC) and partial WTC were used to investigate the temporal and spatial variability of TWS. Several studies have applied the PCA method to investigate TWS patterns in different regions, like South America (Frappart et al., 2013), Africa (Ramillien et al., 2014), Australia (Ramillien et al., 2014; Rieser et al., 2010) and China (Kang et al., 2015; Zhao et al., 2015). Although the PCA analysis of TWS in China showed spatiotemporal patterns based on EOFs (Kang et al., 2015) and emphasised changing TWS patterns by the GRACE error reduction (Zhao et al., 2015), the strengths of relationships between different EOF patterns of TWS and climate factors at different scales are still largely not explored.

In next section, the details of data and method were provided. In the results part, spatiotemporal characteristics of TWS over the East China was characterized based on local wind intensity and Asian monsoons, and ENSO at intra- and inter-annual scales. In the discussion, shifting TWS distribution over the East China between 2003 and 2015 was explained based on different scaled climate drivers. In the concluding section, the implications and possible future applications of shifting TWS based on this study were summarized.

2. Materials

In this study, multiple satellites products were used to get hydrological variables, and reanalysis datasets to derive meteorological variables and the climate indices. The detailed information of datasets was summarized in Table 1.

Table 1. The description of datasets used in this study.

Products	Variables	Spatial range and resolution	Temporal range and resolution	References

GRACE RL05	TWS	Global, 1×1°	2003-2015, monthly	Tapley et al. (2004)
GLDAS V2.1 NOAH	TWS	60°S-90°N, 180°W-180°E, 1×1°	2000-2018 monthly	(Rodell and Beaudoing, 2017)
TRMM 3B43 V7	precipitation	50°S-50°N, 180°W-180°E, 0.25×0.25°	1998-2016, monthly	Huffman et al. (2007)
MOD 16A2	ET	Global, 0.5×0.5°	2000-2014, monthly	Mu et al. (2011)
ERA-Interim	Wind, specific humidity	Global, 0.7×0.7°	1979-2018, monthly	Dee et al. (2011)
	Asian monsoon indices		2003-2015, monthly	Wang et al. (2001); (Zhu et al., 2005)
	Nino 3.4 SST index		2003-2015, monthly	Rayner et al. (2003)

2.1 GRACE and Global Land Data Assimilation System (GLDAS)

For monitoring TWS based on gravity anomalies, the average of three different gravity solution of GRACE Level-2 Release 05 (RL05) derived from the Jet Propulsion Laboratory (JPL) of National Aeronautics and Space Administration (NASA) (ftp://podaac.jpl.nasa.gov/allData/grace/L2/CSR/RL05), the Center for Space Research (CSR) at University of Texas, Austin (http://www2.csr.utexas.edu/grace) and the GeoforschungsZentrum (GFZ) in Potsdam (http://isdc.gfz-potsdam.de/grace) was used, in the form of Stokes spherical harmonic coefficients (SHCs) up to degree and order 90 for JPL and 60 for CSR and GFZ (Tapley et al., 2004). Wahr et al. (1998) gave the equation of equivalent water height (EWH), which is a measure of TWS based on the SHCs. It can be defined as follow:

$$\Delta\sigma(\theta,\lambda) = \frac{a\rho_{ave}}{3\rho_w}\sum_{n=0}^{\infty}\sum_{m=0}^{n} P'_{nm}(cos\theta)\frac{2n+1}{1+k_n}\left(\Delta C_{nm}cos(m\lambda) + \Delta S_{nm}sin(m\lambda)\right) \quad (1)$$

where θ and λ are the colatitude (i.e., the complementary angle of a given latitude) and east longitude respectively, a and ρ_{ave} are the mean radius and density (around 5517 kg/m^3) of the Earth, ρ_w is the water density (1000 kg/m^3). P'_{nm} is the normalized Legendre function, k_n represents the loading Love number loading, ΔC_{nm} and ΔS_{nm} are the of residual SHCs (i.e. SHCs minus their long-term mean field) at degree *n* and order *m*.

For reducing the estimate errors of gravity anomalies from GRACE, the degree-1 SHCs representing the geocenter motion coefficients were added into the gravity field (Swenson et al., 2008), and the term C20 terms were replaced by the results from Satellite Laser Ranging (SLR), because the near-circular orbit of GRACE satellite was not sensitive to the second-order coefficient C20 term (Cheng and Tapley, 2004). The Gaussian filtering with a radius of 350 km and the detriping procedure were applied to reduce the uncertainties of SHCs at high degrees (Swenson and Wahr, 2006). In this study, the arithmetic mean of JPL, CSR and GFZ solutions was chosen to reduce the noise of gravity field solutions within the available scatter, as recommended by Sakumura et al. (2014). The GRACE data was spanning from January 2003 to December 2015, and missing data were interpolated linearly from the adjacent values of missing months.

For removing the groundwater variation in TWS, the GLDAS Version 2.1 Noah product was applied in this study, available at Goddard Earth Sciences Data and Information Services Center (https://disc.gsfc.nasa.gov/datasets/GLDAS_NOAH10_M_2.1/summary?keywords=GLDAS) (Rodell and Beaudoing, 2017). Since the GRACE TWS includes the soil moisture in all layers, snow content, plant conopy water, surface runoff, reservoir water and groundwater, the GLDAS TWS is the combination of precipitation, ET and runoff, without groundwater variations. The product has the time span from 2000 to 2018 at monthly scale, with a spatial coverage of 60°S-90°N, 180°W-180°E and 1 degree resolution.

2.2 Precipitation and Evapotranspiration

For relating TWS data to precipitation fields, the Tropical Rainfall Measuring Mission (TRMM) Multi-satellite Precipitation Analysis (TMPA) data product 3B43 version 7 was used (https://pmm.nasa.gov/data-access/downloads/trmm). This product was spanning the period from 1998 to 2016 on a monthly scale, with a spatial coverage of 50°S-50°N and a 0.25×0.25° horizontal resolution. Based on the improved algorithm of Mu et al. (2011) for the MODerate Resolution Imaging Spectroradiometer (MODIS), ET for this study was the MOD 16A2 product between 2000 and 2014, with a 0.5×0.5°horizontal resolution, from the NASA EOSDIS Land Processes DAAC website (https://lpdaac.usgs.gov/products/mod16a2v006/) (Running et al., 2017). For spatial consistency between variables, the TRMM precipitation and MOD ET products were smoothed to a spatial resolution of 1×1° to be the same as the GRACE grid.

In addition, previous studies showed that the TRMM product is highly biased and bias correction methods are needed for getting more reliable results (e.g., Biabanaki et al., 2013; Li et al., 2010; Shukla et al., 2019). In this study, the quantile mapping method (Shukla et al., 2019) based on cumulative distribution function (CDF) was used to correct the bias of the TRMM product by using the observed monthly precipitation from multiple stations in south China (precipitation stations were shown in Figure S1). In south China, the TRMM precipitation matched well with the observation, with a high correlation of 0.950 (Figure S2a), indicating the TRMM bias in south China was very small. For the comparison of the precipitation CDF derived from observation and TRMM, the TRMM precipitation was very slightly smaller than the observation for a given CDF value (Figure S2b), indicating there was a very small negative bias of TRMM in south China. After the correction, the correlation between TRMM and observation was raised to 0.954, and the CDF curves of TRMM and observation overlapped, displaying the improvement of the TRMM precipitation. The precipitations in all grids were corrected by using this quantile mapping method, and the TRMM precipitation in the following text refers to the corrected precipitation.

2.3 Moisture flux

For looking at regional water movement, the moisture flux and its divergence, were calculated by multiplying wind (including zonal (u) and meridional (v) wind components, and vertical velocity) to the specific humidity extracted from the ERA-Interim reanalysis dataset (https://apps.ecmwf.int/datasets/data/interim-full-moda/levtype=sfc/), provided by the European Centre for Medium-Range Weather Forecasts (ECMWF) (Dee et al., 2011). The latest dataset was covering the period between 1979 and 2018, with a 0.7×0.7° horizontal resolution.

2.4 Monsoon and ENSO Indices

For linking the climate factors to water dynamic over the East China, three Asian monsoon and ENSO indices were used in this study. Three Asian monsoon indices, including Indian Monsoon (IM), East Asian Monsoon (EAM) and Western North Pacific Monsoon (WNPM), were calculated based on the definition of Wang et al. (2001) and Zhu et al. (2005). According to Wang et al. (2001), the IM index was calculated based on the difference of the 850-hPa zonal winds between a southern region (5°-15°N, 40°-80°E) and a northern region (20°-30°N, 70°-90°E), while the WNPM index was derived from the 850-hPa zonal wind difference between a southern region (5°-15°N, 100°-130°E) and a northern region (20°-30°N, 110°-140°E). In addition, the EAM index was calculated by the differences between 850-hPa and 200-hPa zonal winds (Zhu et al., 2005). The wind dataset was provided by the ECMWF.

Different ENSO indices were proposed to quantify the strength of ENSO events, e.g. Southern Oscillation Index (SOI) (Allan et al., 1991) and Nino 3.4 SST index (Rayner et al., 2003). In this study, the Nino 3.4 SST anomaly index (freely available from the National Climatic Data Center [NCDC] of the National Centers for Environmental Information [NCEI] website, at https://www.ncdc.noaa.gov/teleconnections/enso/indicators/sst/) was used.

3. Methodology

3.1 Principal component analysis

The principal component analysis (PCA) has been widely used to extract modes of spatiotemporal variability in hydrological and climate sciences (e.g., Awange et al., 2014; Biabanaki et al., 2013; Rieser et al., 2010). In particular, the PCA was applied to decompose the spatiotemporal TWS data sets into modes of empirical orthogonal functions (EOFs) and principal components (PCs) corresponding to the spatial and temporal variations, respectively. The TWS data sets derived from GRACE can be denoted as $X = (x_{ij})$, with $i = 1, \ldots, p; j = 1, \ldots, n$. The n column vectors of the matrix X represent spatial grid TWS values at interested area for a particular month, while the p raw vectors are temporal TWS variation at a particular grid locations.

The PCA decomposes the matrix X to obtain corresponding EOFs and PCs, denoted as:

$$X = ZA^T \tag{2}$$

where $\boldsymbol{Z}$ is a $p \times n$ matrix, derived through an eigenvalue decomposition of the matrix HH^T, and the columns of $\boldsymbol{Z}$ represent the EOFs of the original TWS. Once the EOFs have been obtained, the time coefficient matrix $\boldsymbol{A}$ can also be obtained through the equation (2). The column vectors of matrix A represent the corresponding temporal PCs. The first few largest EOFs/PCs are commonly selected, as it reduces the number of variables, while grasping the main characteristics and simplifying the relationship between variables. Note that unlike other PCA studies (Awange et al., 2011; Ramillien et al., 2014), no detrend procedures were applied to the original variable $\boldsymbol{X}$ (i.e., TWS). Additionally, although the rotation procedure has been widely applied to the EOFs, to help better interpreting the results in some studies (Hannachi et al., 2006; Vuille et al., 2000; White et al., 1991), its drawbacks should not be neglected. These drawbacks include non-uniform rotation criterion and the loss of information from the EOFs (Jolliffe, 1989). To avoid such a loss of underlying information of TWS EOFs, no rotation procedures were applied in this study. In addition, the sensitivity of the PCA results will be checked by looking at the residual parts after extracting the principal components to investigate how the main components of the TWS are affected by the residual components of PCA.

3.2 Extraction of different time-scale of variability

Except for the PCA method, the additive model was also applied to decompose the TWS time series into trend, seasonal and residual signals. It can be shown as

$$H = H_t + H_s + H_r \# (3)$$

and

$$H_t = b \times t + c \#$$

$$H_s = A \times cos(\omega t - \varphi) \#$$

where H represents the TWS, and H_t, H_s, H_r are corresponding trend, seasonal and residual part of H, respectively; b and c are trend term and intercept term. A, ω, and φ represent amplitude of seasonal variation, frequency and phase. In this study, seasonal variation (here only considering the annual and semiannual signals) and linear trend of the TWS were obtained by applying a nonlinear regression in each grid of the study area.

3.3 Non-stationary relationship between TWS and climate variability

The wavelet transform coherence (WTC) here was proposed by Torrence and Webster (1999), and it was modified and improved by different researchers (Grinsted et al., 2004; Lachaux et al., 2002). Based on (Grinsted et al., 2004), the continuous wavelet transform (CWT) of two time series X and Y of length N with uniform time step Δt are denoted as $W_n^X(s)$ and $W_n^Y(s)$:

$$W_n^X(s) = \sqrt{\frac{\Delta t}{s}} \sum_{n'=1}^{N} X_{n'} \psi_0 \left[(n' - n) \frac{\Delta t}{s} \right] \tag{4}$$

where n and s are the time index and wavelet scale, respectively. The ψ_0 is generally chosen as the Morlet wavelet, defined as:

$$\psi_0(\eta) = \pi^{-1/4} e^{i\omega_0 \eta} e^{-\eta^2/2}$$

where ω_0 and η represent the dimensionless frequency and time, respectively. In order to keep a good tradeoff between frequency and time, the parameter ω_0 was chosen to be 6 (Müller et al., 2004).

Following Grinsted et al. (2004), the WTC of two time series can be calculated as:

$$R_n^2(Y, X) = \frac{\left| S^m\left(s^{-1} W_n^{XY}(s)\right) \right|^2}{S^m\left(s^{-1} \left|W_n^X(s)\right|^2\right) \cdot S^m\left(s^{-1} \left|W_n^Y(s)\right|^2\right)} \tag{5}$$

where $W_n^{XY}(s)$ is the cross-wavelet spectrum, defined as:

$$W_n^{XY}(s) = W_n^X(s) W_n^Y(s)^*$$

where $*$ indicates the complex conjugate. S^m denotes a smoothing operator in both time and frequency scale. The significance level of WTC is calculated based on the Monte Carlo methods. The phase difference of WTC can be written as:

$$\phi_n(s) = arg\left(S^m\left(s^{-1} W_n^{XY}(s)\right)\right) \tag{6}$$

In addition, the partial WTC is used to calculate the WTC results of two variables after removing their common dependent factor (Mihanović et al., 2009). Assuming the common dependent factor denoted as Z, the partial WTC between X and Y (removing the Z effect) can be defined as

$$PR_n^2(Y, X, Z) = \frac{|R_n^2(Y, X) - R_n^2(Y, Z) \cdot R_n^2(Y, X)^*|^2}{[1 - R_n^2(Y, Z)]^2 \cdot [1 - R_n^2(Z, X)]^2} \#(7)$$

where the $R_n^2(Y, X)$, $R_n^2(Y, Z)$ and $R_n^2(Z, X)$ are the WTC between X and Y, Y and Z, and X and Z, respectively.

4. Results

4.1. Spatiotemporal characteristics of the TWS

Representing 70% of the total TWS variance, two main spatial features of TWS (hereafter called TWS EOF 1 and TWS EOF 2) were extracted using the PCA. Both TWS EOF 1 and EOF 2 (58% and 12% of the TWS variance respectively) showed prominent hot spots (Figure 1a-b). The spatial characteristics of seasonal variation and linear temporal trend of TWS during 2003 and 2015 were consistent with the TWS EOF 1 and EOF 2, respectively (Figure 1c-d). To quantify the similarity between TWS EOF1 (EOF 2) and TWS seasonal variation (linear temporal trend), spatial correlations were estimated: TWS EOF 1 and seasonal variation were significantly correlated at 0.84 ($p << 0.05$), and TWS EOF 2 had a high correlation of 0.95 ($p<<0.05$) with the linear temporal trend. The results indicated that the TWS EOF 1 and EOF 2 represent the seasonal variation and temporal trend respectively.

According to Figure 1, for the TWS seasonal variation (i.e., TWS EOF 1), the strongest annual variation of the TWS was in the Indochinese Peninsula, where existing large annual and inter-annual water variation in response to the Southeast Asian monsoon (Yamamoto et al., 2007). Over China, the seasonal variation in southern region was relatively larger than other regions (Figure 1a and c). For the trend signal, there were three main hot spots over China, indicating increasing trend (yellow spots) and decreasing trend (deeper blue spots) of the TWS (Figure 1b and d). The two increasing hot spots were in the southern (YARB) and western China (around Qinghai-Tibet Plateau [QTP]), whereas the decreasing hotspot was in the NCP (Figure 1b and d). Since the western region was sparsely populated, the demand for water supply and water management would be less pressured, and the East China was chosen as the interested area, with the latitude and longitude range between 20-45°N and 105-125°E.

The seasonal and trend characteristics of TWS without the groundwater variations were shown in the Figure 1e-f (i.e., GLDAS TWS EOF1 and EOF2), explaining around 32% and 23% of the total variance, respectively. The pattern of GLDAS TWS EOF1 was quite similar with the GRACE TWS, with the correlation of 0.67 ($p << 0.05$), and this result reveals that the seasonal TWS variations were less likely to be affected by groundwater variations. However, the increasing trend of GLDAS TWS over the YARB and decreasing trend over the NCP were less obvious than GRACE TWS. Despite the significance, the correlation between GLDAS and GRACE TWS was only 0.34 ($p << 0.05$). The result here indicates that GLDAS have weak information of surface and subsurface runoff variations, and runoff variations in the GRACE data can be important to the unbalance water distribution over East China.

For investigating the contributions of other hydrological components to the unbalance water distribution over the East China, the first- and second-EOFs of precipitation and ET (hereafter called precipitation EOF 1 and EOF 2, ET EOF 1 and EOF 2) were extracted (Figure S3). Precipitation EOF 1 showed a pattern of more precipitation over the YARB, explaining around 48% of the total variances in precipitation (Figure S3a). The seasonal variation of ET shown by the ET EOF 1 had a gradual decrease from south to north China, representing around 88% of the ET total variances (Figure S3c), which was almost twice as much as in precipitation, suggesting potential differences in climate drivers of precipitation and ET. The ET was mainly impacted by temperature and air circulation including wind speed and relative humidity, which mainly changed seasonally, except for relatively small long-term variations (Gao et al., 2006). However, unlike ET, the climate drivers of precipitation over the East China involved different monsoons, ENSO and local climate conditions, leading to less seasonality in precipitation (Chan and Zhou, 2005; Gao et al., 2017).

For the trend signal of precipitation and ET (i.e., precipitation EOF 2 and ET EOF 2), there was more precipitation and less ET over the YARB, but less precipitation and more ET over the NCP (Figure S3b and S3d). The results further demonstrated that the wet southern region was getting wetter, and the dry northern region was getting drier over the East China. Also, the TWS, precipitation and ET EOF2 (Figure 1b, S3b and S3d) suggested that there was a dividing line around 33°N to separate the different trend of hydrological variables, and over the two sides of the dividing line, there was an unbalance water distribution with complex underlying mechanisms. For measuring the consistency of seasonal and trend pattern of precipitation (ET) and TWS derived from GRACE, the spatial correlations of their EOFs were computing. The spatial patterns of precipitation and ET were consistent with the TWS. For EOF 1, the correlation of TWS and precipitation is 0.38 ($p << 0.05$) and correlation of TWS and ET is 0.45 ($p << 0.05$). For the EOF 2, they are 0.44 ($p << 0.05$) and -0.47 ($p << 0.05$). The results indicated that the precipitation and ET are related to the spatiotemporal dynamics of the unbalance water distribution pattern over the

East China.

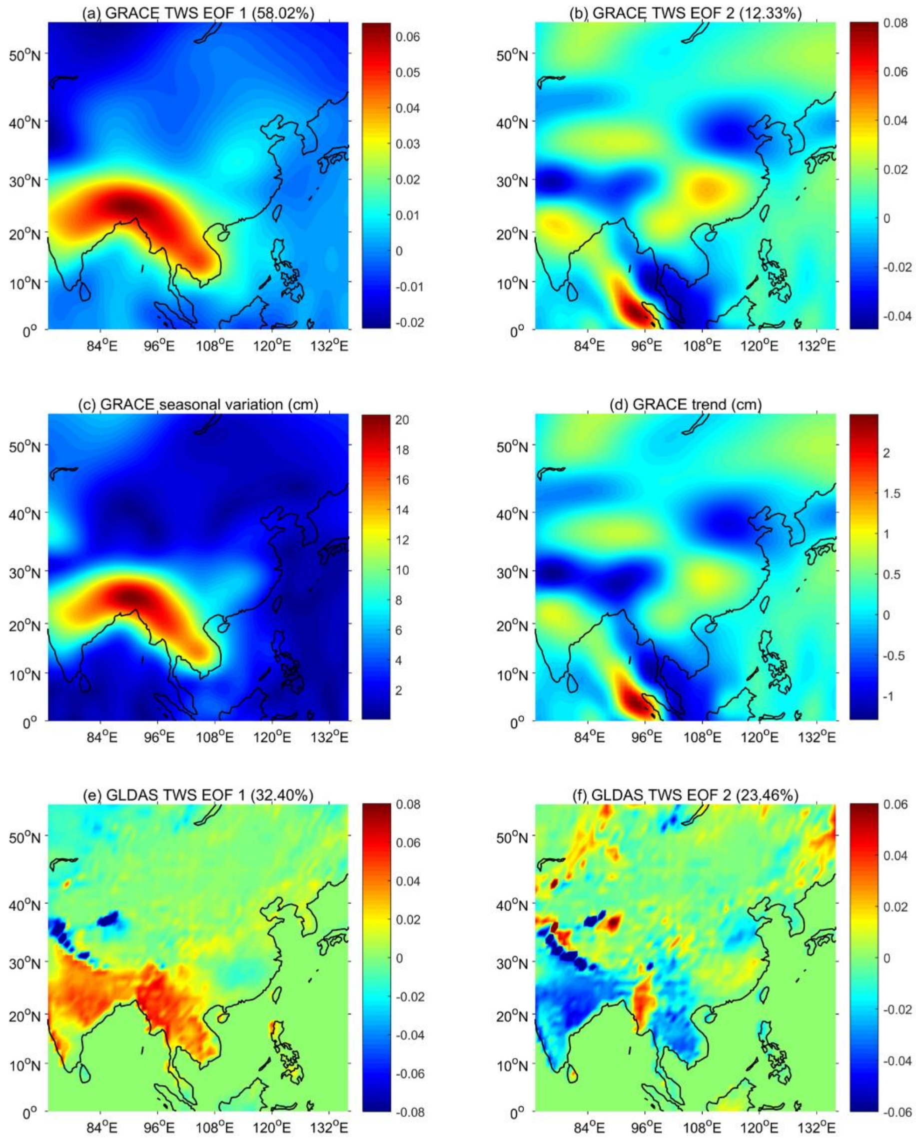

Figure 1. (a-b) The TWS EOF 1 and EOF 2 based on the PCA. (c-d) The spatial distribution of the TWS seasonal variation and temporal trend, respectively. Note that when comparing figures, the scales of figures in top and bottom are different for readability purpose.

To explore the variability and underlying drivers of the TWS spatial EOFs, the corresponding PCs of TWS modes 1 and 2 (hereafter called TWS PC 1 and PC 2) were extracted, and displayed in Figure 2. The TWS PC 1 showed annual periodicity, which was here shown not to be constant, with lower intensity between 2009 and 2010, for instance (Figure 2a). This lower intensity of the seasonal signal in TWS mode 1 thus appeared consistent with the 2009-2010 drought over the YARB (Tang et al., 2014). For the TWS PC 2, there was a prominent linear increase, indicating that the unbalance water distribution shown by the TWS EOF 2 was getting more pronounced year after year since 2003 (Figure 2a). This was therefore consistent with both the increasing rate over the YARB and the decreasing rate over the NCP (Figure 2b), which were both accelerating from 2003 to 2015, hence putting more pressure on the China’s water management.

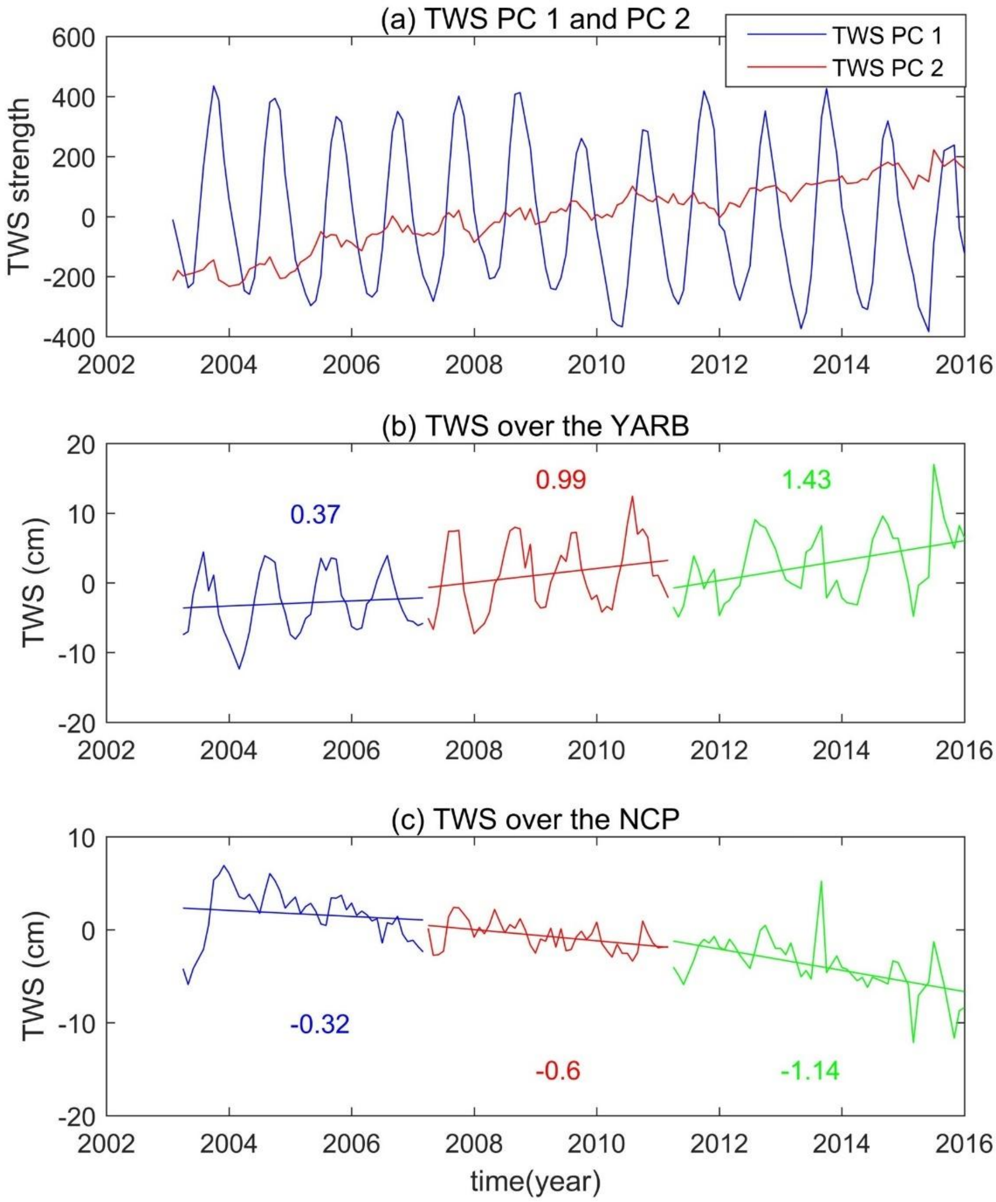

Figure 2. (a) The TWS PC 1 and 2. (b-c) TWS time series over the YARB and the NCP, respectively. Colored values represent the trend rates during period of 2003-2007 (blue), 2007-2011 (red) and 2011-2015 (green), as estimated through linear regression.

For illustrating the increasing and decreasing trends, the TWS time series over the YARB and the NCP regions were extracted (Figure 2). For the whole time series, TWS kept increasing over the YARB, and decreasing over the NCP from January 2003 to December 2015. To explore the TWS changing rate over time, break-point detection algorithm (Muggeo, 2003) was applied, and two break-points, which may be linked to ENSO events, are identified over the YARB region in 2007 and 2011 (Figure S4a). A strong La Nina and moderate La Nina event were indeed reported in 2007 and 2011, respectively (Figure S5), which could lead to abrupt changes in precipitation and temperature (Chen et al., 2016; Fang et al., 2017; Nicholls et al., 1996), and thus TWS. Therefore, the whole period was divided into three parts: from January 2003 to February 2007 (hereafter called Period 1), from March 2007 to February 2011 (hereafter called Period 2) and from March 2011 to December 2015 (hereafter called Period 3). The increasing rates of TWS over the YARB in three periods were 0.37 $cm.yr^{-1}$., 0.99 $cm.yr^{-1}$ and 1.43 $cm.yr^{-1}$, whereas the TWS over the NCP was decreasing with a rate of 0.32 $cm.yr^{-1}$, 0.6 $cm.yr^{-1}$ and 1.14 $cm.yr^{-1}$ in the Period 1, 2 and 3, respectively (Figure 2b-c). This result was consistent with the finding derived from the temporal TWS PC 2, revealing that the YARB wetting and the NCP drying were becoming more and more pronounced during 2003 and 2015. In addition, there are also two break-points of TWS over the NCP in 2007 and 2014 (Figure S4b). Although the break-points of TWS in the YARB and NCP were slightly different, they provided the same results in term of water situation over the East China.

Given this severe situation of the water redistribution over the East China, it is of primary important to explore its underlying drivers, which can be useful to predict the season ahead water situation in the future, so that seasonal water management policies can be developed.

4.2 The underlying climate drivers of TWS spatial patterns

Atmospheric circulation over the East China has direct impacts on water distribution pattern through precipitation and evaporation (Liu et al., 2017; Xu et al., 2015), and the upward and downward motions related to regional convergence and divergence associated with wetter or drier conditions, respectively (Li, 1999; Zhang et al., 2017; Zhou and Yu, 2005). To explore the impact of atmospheric circulation over the East China, meridional cross-sections of wind circulations, moisture flux and divergence averaged over the region between 105^{o} and 120^{o}E in summer (JJA) and winter (DJF) were displayed in the Figure 3. For the wind circulation, there was an upward convergence between 25 and 33^{o}N (i.e., the YARB) in summer, and a downward divergence between 33 and 43^{o}N (i.e., the NCP) in winter (Figure 3). The Hadley-type circulation could also be observed, transporting energy from the Equator to around 33-degree latitude (Figure 3b), which was consistent with the dividing line of the unbalance water distribution (Figure 1d). The ascending branch of the Hadley-type circulation moved from the Equator in winter to around 25-degree north latitude in summer (Figure 3), creating excessive precipitation over the region of 25-33°N, and this could partially explain the wetting trend over the YARB. The moisture flux circulation showed similar pattern with the wind circulation below 500 hPa and there was no moisture in the upper-troposphere (Figure 3). For the moisture flux divergence, there was a convergence and divergence between 20° and 30°N below 820 hPa in summer and winter respectively (Figure 3), producing more (less) precipitation in summer (winter) over the YARB.

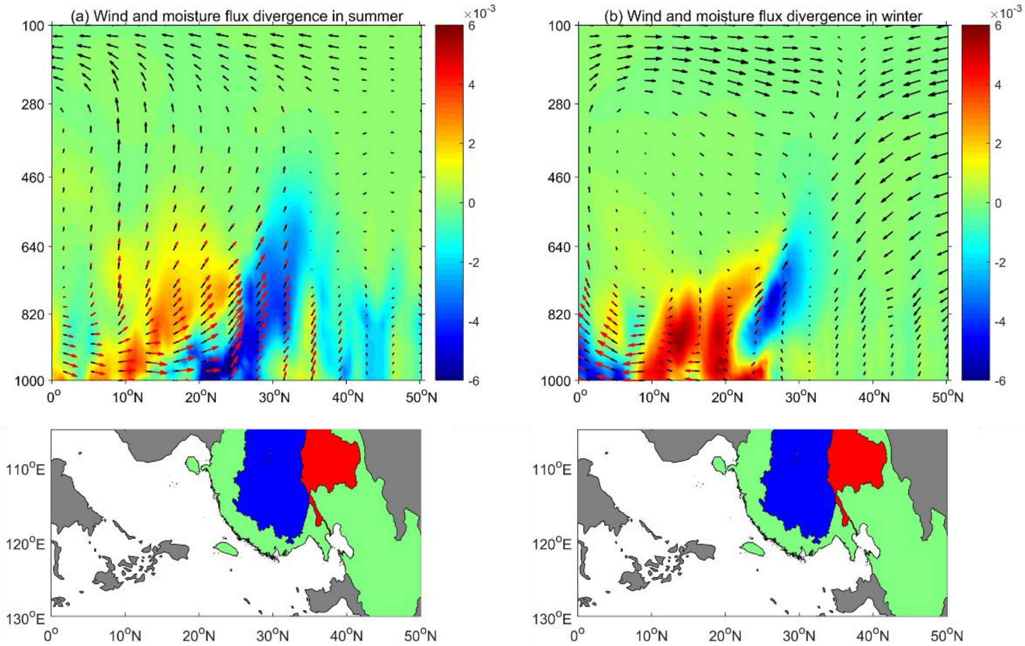

Figure 3. (a-b) The meridional cross-section of wind, moisture flux and divergence over the region (105^{o}-120^{o}E) in summer and winter. Note that the black and red arrow are the wind and moisture flux respectively, and the shaded area represents the moisture flux divergence. The corresponding administrative boundary of the region (105^{o}-130^{o}E, 0^{o}-50^{o}N) is added to the bottom of the wind profile. The green shaded

area is China, and the blue and red shaded area represent the YARB and YERB boundary, respectively.

In addition, to explore the temporal variation of TWS distribution affected by the atmospheric circulation over the East China at different temporal scales, the wind intensity was extracted over this region. The WTC analysis between TWS PC 1 and the wind intensity suggested that wind intensity mainly contributed to the annual and semiannual (hereafter called intra-annual) signals of the TWS PC 1 with time lags of ~6 months and ~4.5 months, respectively (Figure 4a). The WTC analysis between TWS PC 1 and three monsoon indices revealed that IM and WNPM contributed significantly to TWS PC 1 at both intra-annual and inter-annual (i.e., 2-4 years) scale during the whole period, with a time lag of ~2 months (Figure 4b-c), whereas the EAM affected the intra-annual TWS signals significantly during the whole period with a time lag of ~2 months, but only contributed the inter-annual signals after 2010 (Figure 4d).

Apart from the atmospheric circulation and monsoons, ENSO also played an important role in the water redistribution over the East China, but at longer time scale than atmospheric circulation and Asian monsoons. Based on the WTC, there was a significant relationship between TWS PC 1 and ENSO at 2-4 year time scale with a time lag ~4 months (Figure 4e). Due to the short period of the TWS, the relationship was significant only between 2006 and 2012; and this limitation could only be overcome when the TWS time series get longer. To disentangle the influence of Asian monsoons and ENSO on TWS PC 1, the partial WTC were used (Ng and Chan, 2012; Figure 5). The results showed that ENSO had non-significant impact on TWS PC 1 when removing the Asian monsoons effect, indicating that the ENSO indirectly affected TWS variability through the Asian monsoons (Figure 5a-c). Similarly, the significant relationships between Asian monsoons and TWS at inter-annual scale were weakened after removing the ENSO effect (Figure 5d-f).

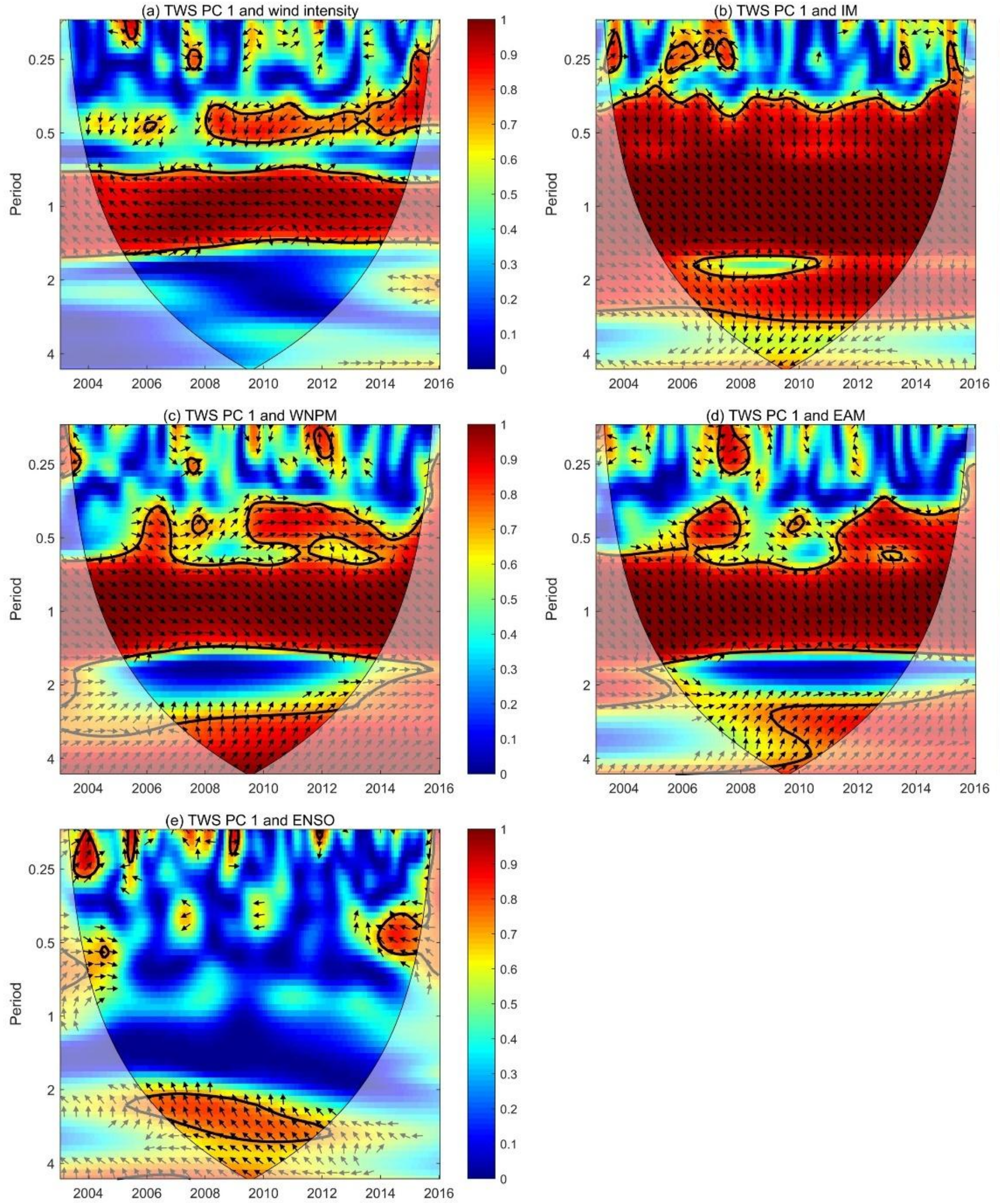

Figure 4. The WTC analysis of the TWS PC 1 and the wind intensity (a) over the East China, Asian monsoons (b, c and d) and ENSO (e). The thick black contour represents the 5% significance level against the red noise. The thin black line is the boundary of the cone of influence (COI), that is, the edge effects caused by zero-padding effect. The phase lag is denoted by the arrow directions (right (left) is 0 (180) degree phase lag; up (down) is 270 (90) degree phase lag).

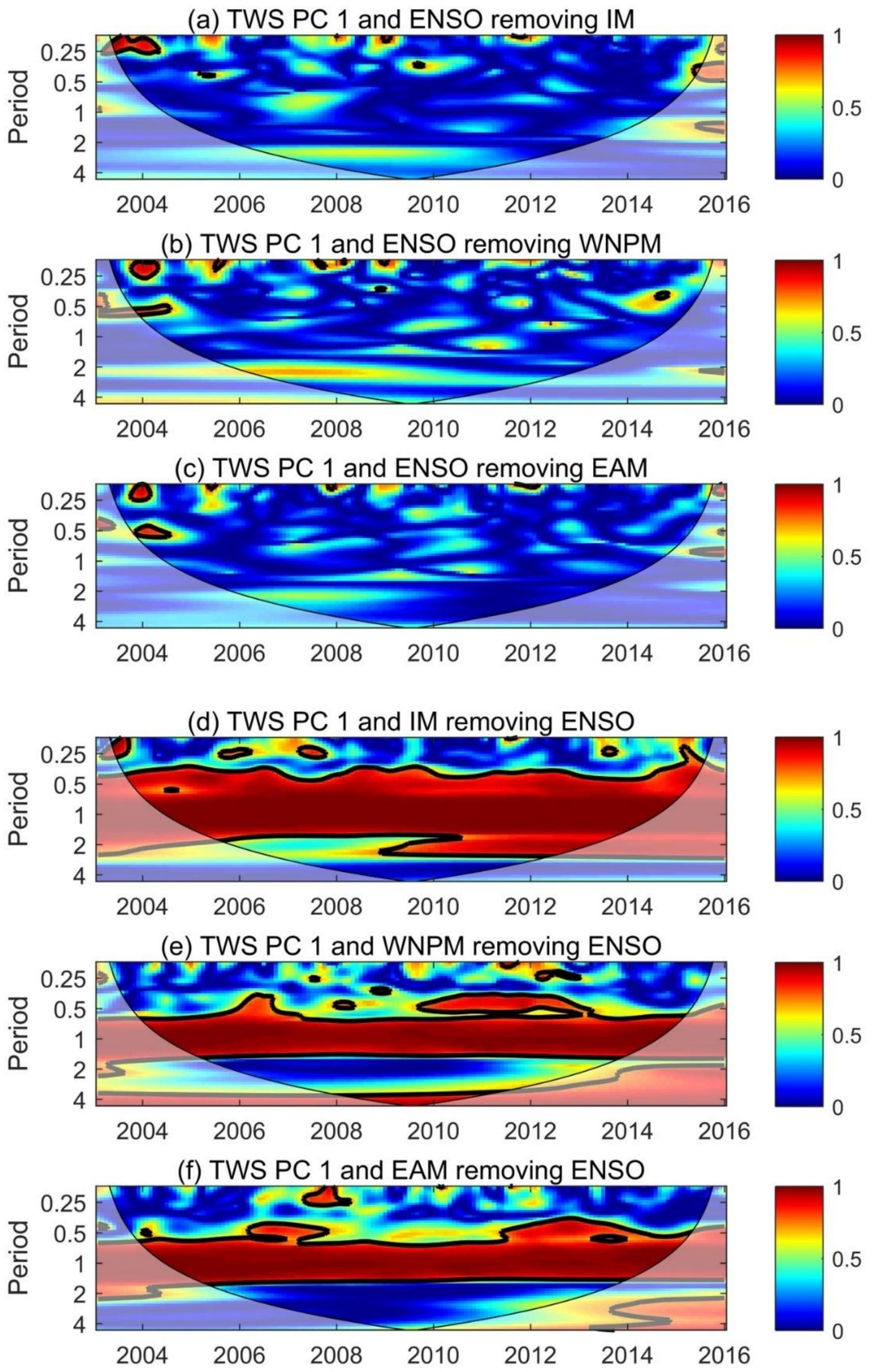

Figure 5. (a-c) Partial WCT of TWS PC 1 and ENSO removing the Asian monsoons effect; (e-f) partial WCT of TWS PC 1 and Asian monsoons removing the ENSO effect. The cross-hatching represents regions inside the COI and the thick contour means the 95% significance level.

To avoid the interaction between different scaled signals, a multilevel wavelet analysis was performed using the Daubechies wavelet to separate the TWS PC 1 into two components based on the above WTC results, *i.e.* intra-annual and inter-annual signals. For the Daubechies's orthogonal wavelets, after testing different levels, the level 5 (db5) was used in this study, as it provides a good approximation in time and scale domain (Percival and Walden, 2000). The intra-annual and inter-annual signals have then been derived from the detail and approximation parts of the db5 wavelet, respectively, which were then used to examine the relationship with different climate factors *via* cross-correlation in different time scales. The intra-annual signals of TWS PC 1 and the wind intensity had negative relationship with a correlation coefficient of -0.49 ($p \ll 0.05$) and with a time lag shorter than a month (Figure 6a).

For Asian monsoons, there were time lags at the intra-annual scale (Figure S6a-c), and the impacts of IM, WNPM and EAM on TWS lagged by 2 months, 1 month and 2 months, respectively, which were consistent with the WTC results (Figure 4b-d). Significant correlations between intra-annual TWS PC 1 and Asian monsoons were obtained after correcting the time lag: 0.94 for IM ($p \ll 0.05$), 0.87 for WNPM ($p \ll 0.05$), 0.88 for EAM ($p \ll 0.05$; Figure 6b-d). The different time lag of different monsoons might be attributed to their characteristics. IM is associated with the north-south thermal contrast between heated Asian land and cool Indian Ocean, while the EAM is related to the east-west thermal contrast between the Asian land and Pacific Ocean (Li and Hsu, 2018). The IM and EAM, induced by land-ocean contrast, are typical continental monsoons, while WNPM associated with the hemispheric asymmetric SST gradients is a kind of oceanic monsoon (Li and Hsu, 2018). The impacts of continental monsoons, IM and EAM, were slower than the oceanic monsoon (i.e., WNPM) by nearly 1 month. In summary, although time lag existing, the Asian monsoons could be significant contributors to water redistribution over the East China.

Compared with the wind intensity and Asian monsoons, the ENSO events were more likely to affect lower frequency variances (i.e., inter-annual scale) of the TWS. The results showed that the TWS PC 1 was negatively correlated with the ENSO at inter-annual (2-4 year) time scale (-0.41, $p \ll 0.05$) with 4 months' time lag (Figure 5e and Figure S6d). The time lag revealed that SST variation in Pacific Ocean takes time to affect the variation of atmospheric circulation, precipitation and, thus, TWS over the East China.

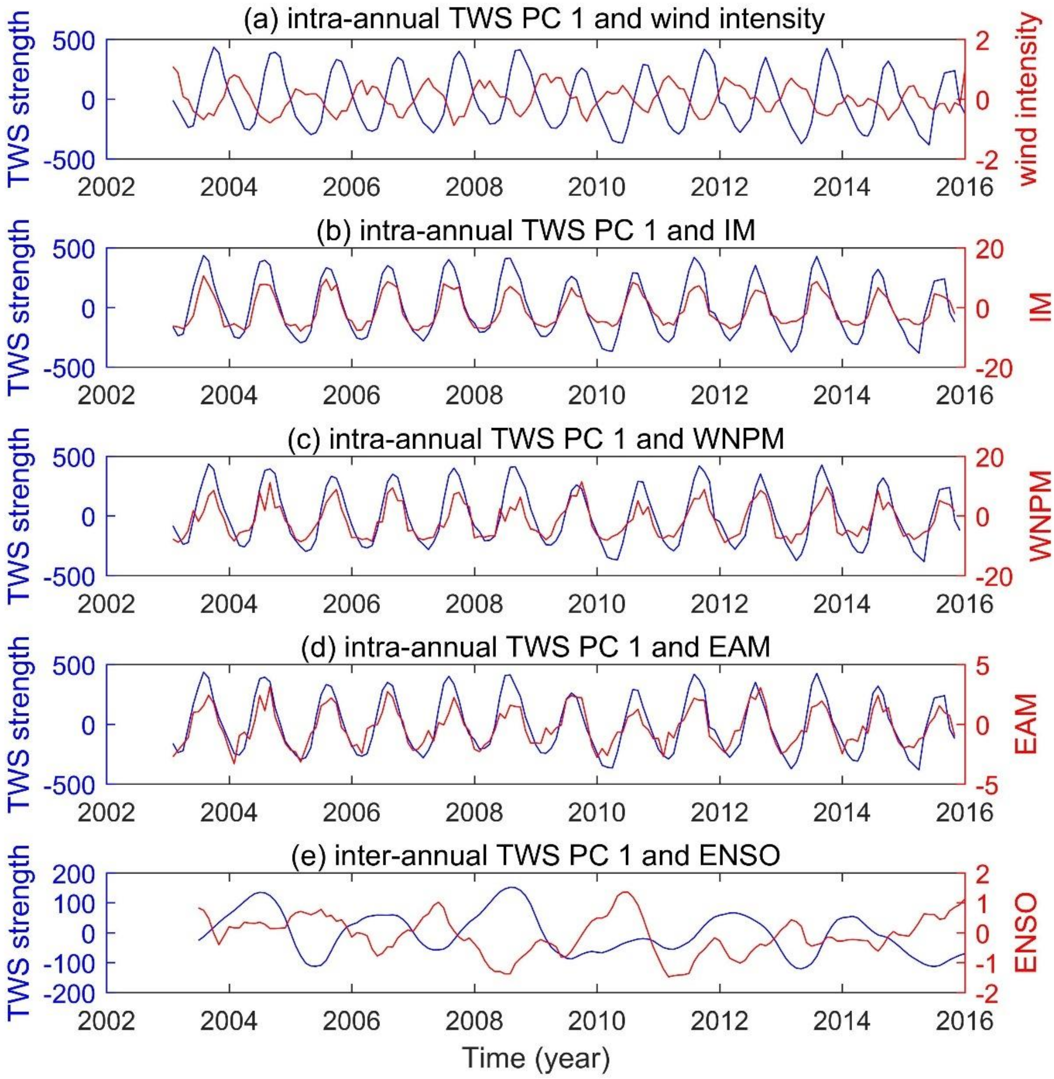

Figure 6. The TWS PC 1 against the wind intensity (a) and IM (b), WNPM (c) and EAM (d) on intra-annual scale and ENSO (e) on inter-annual scale.

As mentioned above, the TWS PC 1 can be decomposed into intra-annual and inter-annual component (i.e., 2-4 year), which can be mainly affected by wind intensity and Asian monsoons, and ENSO respectively. To further explore the relationships between different climate factors and seasonal TWS signals on different time scales, Pearson, Kendal, Spearman and Generalized least square (GLS) correlation were used apart from cross-correlation (Table 2). The four measures were used to qualify the robust of correlation results. The Pearson correlation is the most widely used method, with several assumptions including normal distribution, linearity and homoscedasticity, whereas the Kendal and Spearman correlations are nonparametric approaches based on ranks, with less assumptions than the Pearson correlation. The Kendal and Spearman correlations only assumes that the data should be ordinal, and without any assumptions for distribution. For the GLS correlation, the autocorrelation effects are adjusted. According to the Table 2, on the intra-annual scale, Asian monsoons contributed most, especially the IM and WNPM, whereas ENSO had significant contribution to inter-annual TWS variability. Focusing on the time lags, it was the largest for tele-connected ENSO events, medium for regional Asian monsoons and there was no time lag for local wind intensity, indicating that the response time of TWS to climate variability increased with the increase of spatial scale. Additionally, for the methods calculating correlations, Pearson correlations performed best, but the results were still significant when applying stricter correlation methods including Kendal, Spearman and GLS correlations, which fully proved the validity of our results.

Table 2. Cross-correlation maxima with corresponding time lag, Pearson, Kendal, Spearman and GLS correlation (corresponding p-value) between TWS PC 1 and different climatic factors in intra- and inter-annual scales. Note that the wind intensity and Asian monsoon are correlated with the intra-annual signals of TWS PC 1, while the ENSO is linked to the inter-annual signals.

	Cross-correlation/time lag (month)	Pearson correlation	Kendal correlation	Spearman correlation	GLS correlation
Wind intensity	-0.49/0 (p<<0.05)	-0.49 (p<<0.05)	-0.31 (p<<0.05)	-0.44 (p<<0.05)	-0.11 (p<<0.05)
IM	0.94/2 (p<<0.05)	0.52 (p<<0.05)	0.32 (p<<0.05)	0.50 (p<<0.05)	0.38 (p<<0.05)
WNPM	0.87/1	0.71	0.44	0.65	0.43

	(p<<0.05)	(p<<0.05)	(p<<0.05)	(p<<0.05)	(p<<0.05)
EAM	0.88/2 (p<<0.05)	0.41 (p<<0.05)	0.23 (p<<0.05)	0.36 (p<<0.05)	0.26 (p<<0.05)
ENSO	-0.41/4 (p<<0.05)	-0.31 (p<<0.05)	-0.23 (p<<0.05)	-0.37 (p<<0.05)	-0.31 (p<<0.05)

For investigating the sensitivity of the GRACE EOF results, the residual part (Figure 7a), accounting for 30% of the total variance, was added to the seasonal signal (EOF1, Figure 7b) and trend signal (EOF2, Figure 7c). After adding the residual signal, the seasonal and trend pattern still matched well with the original seasonal and trend pattern (Figure 1a-b), with a correlation of 0.967 ($p \ll 0.05$) and 0.970 ($p \ll 0.05$), respectively. This indicated that seasonal and trend signal were stable, which was not likely to be affected by the residual part.

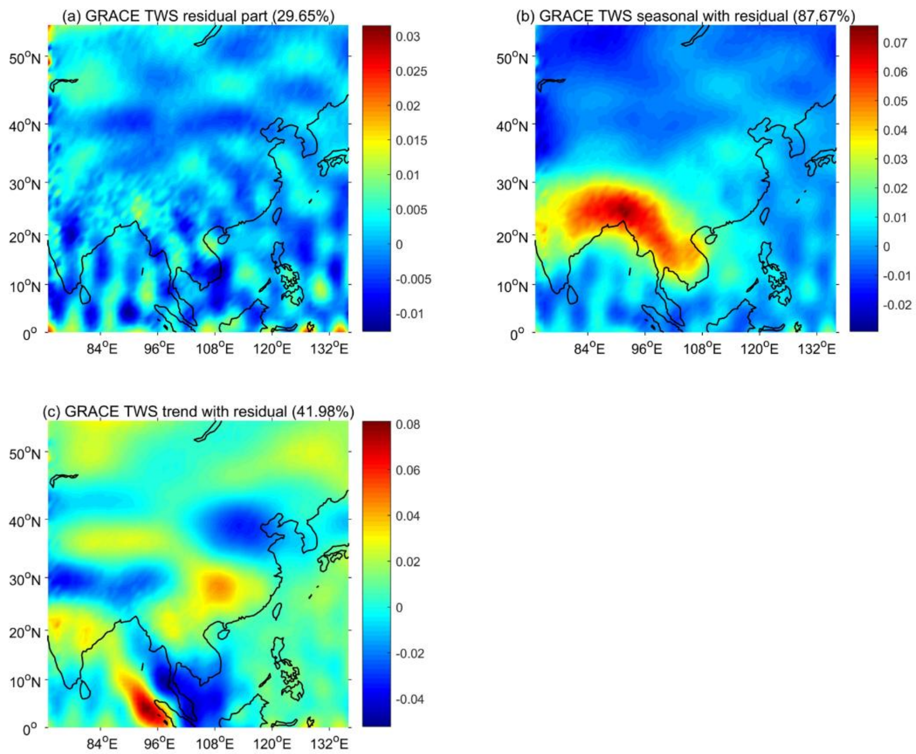

Figure 7. (a) The residual part of GRACE TWS EOF analysis. (b-c) the seasonal signal and trend extracted using EOF analysis, but combined with residual part.

5. Discussion

The aim of this study is to figure out the regional water shifting pattern over the East China, and its corresponding climate drivers on different time scales. The unbalance water distribution between south part and north part of the East China was found, showing that the YARB was wetting, while the NCP was drying during 2003 and 2015. Moreover, the regional unbalance water distribution pattern was found to be significantly linked with the local wind intensity and Asian monsoons on the intra-annual scale, and the ENSO on the inter-annual scale through the modulation of Asian monsoons.

5.1. Spatial characteristics of the TWS

The TWS over the East China showed two main spatial characteristics (i.e., TWS EOF 1 and EOF 2), interpreted as the seasonal and trend variances, respectively (cf. Section 4.1). Specifically, the TWS EOF 1 revealed that the water resources were characterized by more in the south and less in the north over the East China (cf. Section 4.1). Even worse was that the wet region (NCP) became wetter, and dry region (YARB) became drier (cf. Section 4.1). Moreover, both the increasing and decreasing trend were becoming more pronounced year after year during 2003 and 2015.

Given the above results, the uneven distribution of water resources between south and north part of the East China is expected to be aggravated. Furthermore, this kind of water shifting will continue until the end of 21st century according to Fifth Assessment Report of the Intergovernmental Panel on Climate Change (Pachauri et al., 2014). This water situation will intensify both floods and droughts, affecting water demand in industry, agriculture, daily life and ecology over the East China (He et al., 2014). The severe underground water deficit over the NCP is a kind of response to the droughts induced by the water shifting (Du et al., 2014). Therefore, new water management policies, such as the south-north water diversion project (for details: https://nsbd.mwr.gov.cn), should be proposed to solve or mitigate the water problems brought by the water shifting between the YARB and NCP since the water problems would be getting worse and worse.

5.2 Underlying climate mechanism of TWS spatial characteristics

The spatial characteristic of the TWS could result from various climate factors, including local atmospheric circulation, regional monsoons, and ENSO events, as well as different climate factors had different contributions to water distribution over the East China at different time scales. Generally, different scaled seasonal variations in climate factors could lead to the corresponding TWS variations, and other trend changes would also lead to trend variation of the TWS signals. For seasonal variability, climate factors and TWS can be divided into intra-annual and inter-annual parts. It was found that atmospheric circulation and Asian monsoons, showed significant intra-annual cycles, primarily impacting the intra-annual signals of the TWS, while the inter-annual variation was related to ENSO events, *via* modulations of the Asian monsoons, with around 4 months-time delay. This delayed response of the TWS to ENSO over the East China was consistent with other studies, such as Zhang et al. (2015), who found a link between TWS in the YARB and ENSO with a time lag of around 7-8 months. Different time delay may be attributed to the different land surface effects including the water recharge process and topography in different regions, revealing that the response time of TWS over China to ENSO was various in different regions.

Apart from seasonal variations, climate factors also had trend changes, which could partially explain the spatial pattern of the TWS trend variability. It was found that the ENSO events have been strengthened significantly since 1970s (Ding et al., 2009; Wang, 2001). For example, the 1982/1983 and 1997/1998 El Nino event were the two strongest events during 1950 and 2015, and 1990-1994 was the long periods with positive SST anomalies over the Nino 3.4 region (Figure S5), revealing the intensified trend of the ENSO events, which may lead to modulations in the Asian monsoons on inter-annual timescales (Li and Hsu, 2018).

Focusing on the teleconnection between ENSO and Asian monsoons, numerical studies have been proposed for the recent years, including IM (Ashok et al., 2004; Kucharski et al., 2007; Kumar et al., 1999), WNPM (Chou et al., 2003; Wang and Chan, 2002) and EAM (Wang and Li, 2004; Wang, 2002). Among different Asian monsoons, the relationship between ENSO and IM has been most widely discussed. The anticorrelations between ENSO and IM have been found by numerous studies (Kripalani and Kulkarni, 1997; Krishnamurthy and Goswami, 2000; Kucharski et al., 2007). However, Kumar et al. (1999) suggested that the weakening relationship between IM and ENSO had broken down due to the shift in the Walker circulation and enhanced land-sea gradient. Moreover, other climate events like Indian Ocean dipole (IOD) can also reduce the impacts of ENSO events on IM (Ashok et al., 2001).

Despite some skepticism about the anti-correlations between ENSO and IM, the weakening trend of Asian monsoons has been found in many studies (Bollasina et al., 2011; Miao et al., 2017; Wang, 2001), which have been shown to be related to changes in snow cover (Kripalani et al., 2003). With the rising temperature, there is more snow melting, increasing soil moisture and reducing the heating field of the land, and thus leading to the decline of the thermal contrast between Asian land and Pacific Ocean over the Asian monsoon region, so called the Asian monsoon weakening (Kumar et al., 1999). The weakening of the summer Asian monsoon caused that the warm and humid air does not have enough energy to proceed northward (Ding et al., 2008). Meanwhile, the SST increasing over the tropical eastern Pacific strengthens the Hadley-type circulation regionally (Chen et al., 2002), bringing more summer precipitation over the YARB and causing severer dry condition over the NCP region.

6. Conclusion

This study clearly showed the regional shifting pattern over the East China, and the different contributions of climate factors to this pattern on different time scales. Based on the PCA method, the two main spatial characteristics (i.e., TWS EOF 1 and EOF 2) of the TWS over the East China were extracted, and were perfectly consistent with the seasonal variation and temporal trend distribution of TWS, respectively. which was different from the findings shown by Kang et al. (2015). The unbalance water distribution from the EOF 2 was interpreted as a seasonal signal (Kang et al., 2015), while here the EOF 2 unbalance pattern was demonstrated to be the long-term variability between 2003 and 2015 based on the high consistency between trend distribution and EOF 2.

The TWS EOF 1 showed uneven TWS distribution, more in the south and less in the north part of the East China, while the TWS EOF 2 revealed that increasing trends over the YARB, and a decreasing trend over the NCP. Moreover, the corresponding TWS PC 1 and PC 2 gave the temporal variance of these two spatial patterns, showing the periodicity of the seasonal signals and the acceleration of the trend, respectively. The accelerating trend change was consistent with the trend analysis of the TWS time series over the YARB and the NCP. The increasing and decreasing hot spots were linked to the atmospheric circulation over the East China, in particular the seasonal movement of the Hadley-type circulation, leading to ascending air favoring the moisture convergence, and thus wetter conditions over the YARB, while driving subsiding air, divergence and dry conditions over the NCP.

The unbalance water distributions over the YARB and NCP were consistent with the previous studies (e.g., Kang et al., 2015; Zhao et al., 2015), but the underlying climate mechanisms of the unbalance pattern were largely unexplored in the previous studies. In this study, various climatic factors were used for investigating the underlying climate drivers, and the results showed that they contributed differently to TWS variability on intra-annual and inter-annual scales. According to the Table 2, the wind intensity was negatively correlated (-0.49) with the TWS PC 1 on the intra-annual scale. The weakened wind brought less moisture from the south to the north China, and thus this wind leads to more summer precipitation over the YARB and causes severer dry condition over the NCP region. Apart from the wind intensity, the Asian monsoons and ENSO had significantly positive delayed impacts on the intra-annual and inter-annual signals with a correlation around 0.9 (1-2 month delay) and 0.41 (4 months delay), respectively. For the trend variation, it could be partly explained by a regional strengthening of the Hadley-type circulation by the combination of the strengthening of the ENSO events and the weakening of the Asian monsoons. These kind of climate variabilities can also lead to the water shifting in different regions.

Our research provided a profound understanding of dynamics between spatiotemporal water variability over the East China and local atmospheric circulation combined with Asian monsoons and ENSO on different time scales. This study could therefore be used to improve the performance of future hydrological-impact studies based on seamless climate prediction over the East China. Ultimately, these results should be integrated in decision-making process to take measures in advance for large scaled water problems such as regional droughts. Thus, the method used for this study can be also applied in other regions with significant water shifting, and it can help promoting sustainable and resilient regional water future planning in these regions.

Acknowledgements

Q. He performed data processing, wrote and revised the manuscript. K. P. Chun designed the study, collected data, undertook the analysis and revised the manuscript. B. Dieppois and N. Massei commented and revised the manuscript. Thanks to Q. Chen and H. S. Fok for providing data.

Funding

This study is supported by the Hong Kong Baptist University Faculty research Fund (FRG1/1617/005, FRG2/1617/082, FRG2/1516/085), the National Natural Science Foundation of China (NSFC, No. 41674007 and No. 41374010).

Reference

Allan, R.J., Nicholls, N., Jones, P.D., Butterworth, I.J., 1991. A Further Extension of the Tahiti-Darwin SOI, Early ENSO Events and Darwin Pressure. Journal of Climate, 4(7): 743-749. DOI:10.1175/1520-0442(1991)004<0743:afeott>2.0.co;2

Ashok, K., Guan, Z., Saji, N.H., Yamagata, T., 2004. Individual and Combined Influences of ENSO and the Indian Ocean Dipole on the Indian Summer Monsoon. Journal of Climate, 17(16): 3141-3155. DOI:10.1175/1520-0442(2004)017<3141:iacioe>2.0.co;2

Ashok, K., Guan, Z., Yamagata, T., 2001. Impact of the Indian Ocean dipole on the relationship between the Indian monsoon rainfall and ENSO. Geophysical Research Letters, 28(23): 4499-4502. DOI:10.1029/2001gl013294

Awange, J.L. et al., 2011. On the suitability of the 4°×4° GRACE mascon solutions for remote sensing Australian hydrology. Remote Sensing of Environment, 115(3): 864-875. DOI:https://doi.org/10.1016/j.rse.2010.11.014

Awange, J.L. et al., 2014. Characterization of Ethiopian mega hydrogeological regimes using GRACE, TRMM and GLDAS datasets. Advances in Water Resources, 74: 64-78. DOI:https://doi.org/10.1016/j.advwatres.2014.07.012

Biabanaki, M. et al., 2013. A principal components/singular spectrum analysis approach to ENSO and PDO influences on rainfall in western Iran. Hydrology Research, 45(2): 250-262. DOI:10.2166/nh.2013.166

Bollasina, M.A., Ming, Y., Ramaswamy, V., 2011. Anthropogenic Aerosols and the Weakening of the South Asian Summer Monsoon. Science, 334(6055): 502-505. DOI:10.1126/science.1204994

Chan, J.C.L., Zhou, W., 2005. PDO, ENSO and the early summer monsoon rainfall over south China. Geophysical Research Letters, 32(8): L08810. DOI:10.1029/2004gl022015

Chen, J., Carlson, B.E., Del Genio, A.D., 2002. Evidence for Strengthening of the Tropical General Circulation in the 1990s. Science, 295(5556): 838-841. DOI:10.1126/science.1065835

Chen, L.-C., van den Dool, H., Becker, E., Zhang, Q., 2016. ENSO Precipitation and Temperature Forecasts in the North American Multimodel Ensemble: Composite Analysis and Validation. Journal of Climate, 30(3): 1103-1125. DOI:10.1175/JCLI-D-15-0903.1

Cheng, H., Hu, Y., Zhao, J., 2009. Meeting China's Water Shortage Crisis: Current Practices and Challenges. Environmental Science & Technology, 43(2): 240-244. DOI:10.1021/es801934a

Cheng, M., Tapley, B.D., 2004. Variations in the Earth's oblateness during the past 28 years. Journal of Geophysical Research: Solid Earth, 109(B9): B09402. DOI:10.1029/2004jb003028

Chou, C., Tu, J.-Y., Yu, J.-Y., 2003. Interannual Variability of the Western North Pacific Summer Monsoon: Differences between ENSO and Non-ENSO Years. Journal of Climate, 16(13): 2275-2287. DOI:10.1175/2761.1

Dee, D.P. et al., 2011. The ERA - Interim reanalysis: Configuration and performance of the data assimilation system. Quarterly Journal of the royal meteorological society, 137(656): 553-597.

Démurger, S. et al., 2002. Geography, Economic Policy, and Regional Development in China. Asian Economic Papers, 1(1): 146-197. DOI:10.1162/153535102320264512

Ding, Y., Sun, Y., Wang, Z., Zhu, Y., Song, Y., 2009. Inter-decadal variation of the summer precipitation in China and its association with decreasing Asian summer monsoon Part II: Possible causes. International Journal of Climatology, 29(13): 1926-1944. DOI:10.1002/joc.1759

Ding, Y., Wang, Z., Sun, Y., 2008. Inter-decadal variation of the summer precipitation in East China and its association with decreasing Asian summer monsoon. Part I: Observed evidences. International Journal of Climatology, 28(9): 1139-1161. DOI:10.1002/joc.1615

Domrös, M., Gongbing, P., 1988. Climate Classification and Division of China, The Climate of China. Springer Berlin Heidelberg, Berlin, Heidelberg, pp. 230-257. DOI:10.1007/978-3-642-73333-8_8

Du, T., Kang, S., Zhang, X., Zhang, J., 2014. China's food security is threatened by the unsustainable use of water resources in North and Northwest China. Food and Energy Security, 3(1): 7-18. DOI:10.1002/fes3.40

Fang, Y. et al., 2017. Global land carbon sink response to temperature and precipitation varies with ENSO phase. Environmental Research Letters, 12(6): 064007. DOI:10.1088/1748-9326/aa6e8e

Fok, H.S., He, Q., 2018. Water Level Reconstruction Based on Satellite Gravimetry in the Yangtze River Basin. ISPRS International Journal of Geo-Information, 7(7): 286.

Frappart, F., Seoane, L., Ramillien, G., 2013. Validation of GRACE-derived terrestrial water storage from a regional approach over South America. Remote Sensing of Environment, 137: 69-83. DOI:https://doi.org/10.1016/j.rse.2013.06.008

Gao, G., Chen, D., Ren, G., Chen, Y., Liao, Y., 2006. Spatial and temporal variations and controlling factors of potential evapotranspiration in China: 1956–2000. Journal of Geographical Sciences, 16(1): 3-12. DOI:10.1007/s11442-006-0101-7

Gao, T., Wang, H.J., Zhou, T., 2017. Changes of extreme precipitation and nonlinear influence of climate variables over monsoon region in China. Atmospheric Research, 197: 379-389. DOI:https://doi.org/10.1016/j.atmosres.2017.07.017

Grinsted, A., Moore, J.C., Jevrejeva, S., 2004. Application of the cross wavelet transform and wavelet coherence to geophysical time series. Nonlin. Processes Geophys., 11(5/6): 561-566. DOI:10.5194/npg-11-561-2004

Han, Z. et al., 2019. Assessing GRACE-based terrestrial water storage anomalies dynamics at multi-timescales and their correlations with teleconnection factors in Yunnan Province, China. Journal of Hydrology, 574: 836-850. DOI:https://doi.org/10.1016/j.jhydrol.2019.04.093

Hannachi, A., Jolliffe, I.T., Stephenson, D.B., Trendafilov, N., 2006. In search of simple structures in climate: simplifying EOFs. International Journal of Climatology, 26(1): 7-28. DOI:10.1002/joc.1243

He, C., Zhang, L., Zhang, X., Eslamian, S., 2014. Water Security: Concept, Measurement, and Operationalization, Handbook of Engineering Hydrology. CRC Press, Boca Raton, pp. 561-570. DOI:https://doi.org/10.1201/b16766

Huffman, G.J. et al., 2007. The TRMM Multisatellite Precipitation Analysis (TMPA): Quasi-Global, Multiyear, Combined-Sensor Precipitation Estimates at Fine Scales. Journal of Hydrometeorology, 8(1): 38-55. DOI:10.1175/jhm560.1

Jolliffe, I.T., 1989. Rotation of Iii-Defined Principal Components. Journal of the Royal Statistical Society: Series C (Applied Statistics), 38(1): 139-147. DOI:10.2307/2347688

Kang, K., Li, H., Peng, P., Zou, Z., 2015. Low-frequency variability of terrestrial water budget in China using GRACE satellite measurements from 2003 to 2010. Geodesy and Geodynamics, 6(6): 444-452. DOI:https://doi.org/10.1016/j.geog.2015.12.001

Kripalani, R.H., Kulkarni, A., 1997. Climatic impact of El Niño/La Niña on the Indian monsoon: A new perspective. Weather, 52(2): 39-46. DOI:10.1002/j.1477-8696.1997.tb06267.x

Kripalani, R.H., Kulkarni, A., Sabade, S.S., 2003. Western Himalayan snow cover and Indian monsoon rainfall: A re-examination with INSAT and NCEP/NCAR data. Theoretical and Applied Climatology, 74(1): 1-18. DOI:10.1007/s00704-002-0699-z

Krishnamurthy, V., Goswami, B.N., 2000. Indian Monsoon–ENSO Relationship on Interdecadal Timescale. Journal of Climate, 13(3): 579-595. DOI:10.1175/1520-0442(2000)013<0579:imeroi>2.0.co;2

Kucharski, F., Bracco, A., Yoo, J.H., Molteni, F., 2007. Low-Frequency Variability of the Indian Monsoon–ENSO Relationship and the Tropical Atlantic: The "Weakening" of the 1980s and 1990s. Journal of Climate, 20(16): 4255-4266. DOI:10.1175/jcli4254.1

Kumar, K.K., Rajagopalan, B., Cane, M.A., 1999. On the Weakening Relationship Between the Indian Monsoon and ENSO. Science, 284(5423): 2156-2159. DOI:10.1126/science.284.5423.2156

Lachaux, J.-P. et al., 2002. Estimating the time-course of coherence between single-trial brain signals: an introduction to wavelet coherence. Neurophysiologie Clinique/Clinical Neurophysiology, 32(3): 157-174. DOI:https://doi.org/10.1016/S0987-7053(02)00301-5

Landerer, F.W., Swenson, S.C., 2012. Accuracy of scaled GRACE terrestrial water storage estimates. Water Resources Research, 48(4): W04531. DOI:10.1029/2011wr011453

Li, H., Sheffield, J., Wood, E.F., 2010. Bias correction of monthly precipitation and temperature fields from Intergovernmental Panel on Climate Change AR4 models using equidistant quantile matching. Journal of Geophysical Research: Atmospheres, 115(D10): D10101. DOI:10.1029/2009JD012882

Li, Q., Zhong, B., Luo, Z., Yao, C., 2016. GRACE-based estimates of water discharge over the Yellow River basin. Geodesy and Geodynamics, 7(3): 187-193. DOI:https://doi.org/10.1016/j.geog.2016.04.007

Li, T., Hsu, P.-c., 2018. Monsoon Dynamics and Its Interactions with Ocean, Fundamentals of Tropical Climate Dynamics. Springer International Publishing, Cham, pp. 185-229. DOI:10.1007/978-3-319-59597-9_6

Li, W.-P., 1999. Moisture Flux and Water Balance over the South China Sea During Late Boreal Spring and Summer. Theoretical and Applied Climatology, 64(3): 179-187. DOI:10.1007/s007040050121

Liu, S. et al., 2017. Identification of the non-stationarity of extreme precipitation events and correlations with large-scale ocean-atmospheric circulation patterns: A case study in the Wei River Basin, China. Journal of Hydrology, 548: 184-195. DOI:https://doi.org/10.1016/j.jhydrol.2017.03.012

Long, D. et al., 2014. Drought and flood monitoring for a large karst plateau in Southwest China using extended GRACE data. Remote Sensing of Environment, 155: 145-160.

Luo, Z., Yao, C., Li, Q., Huang, Z., 2016. Terrestrial water storage changes over the Pearl River Basin from GRACE and connections with Pacific climate variability. Geodesy and Geodynamics, 7(3): 171-179. DOI:https://doi.org/10.1016/j.geog.2016.04.008

Miao, Y., Warny, S., Clift, P.D., Liu, C., Gregory, M., 2017. Evidence of continuous Asian summer monsoon weakening as a response to global cooling over the last 8Ma. Gondwana Research, 52: 48-58. DOI:https://doi.org/10.1016/j.gr.2017.09.003

Mihanović, H., Orlić, M., Pasarić, Z., 2009. Diurnal thermocline oscillations driven by tidal flow around an island in the Middle Adriatic. Journal of Marine Systems, 78: S157-S168. DOI:https://doi.org/10.1016/j.jmarsys.2009.01.021

Mu, Q., Zhao, M., Running, S.W., 2011. Improvements to a MODIS global terrestrial evapotranspiration algorithm. Remote Sensing of Environment, 115(8): 1781-1800. DOI:https://doi.org/10.1016/j.rse.2011.02.019

Muggeo, V.M.R., 2003. Estimating regression models with unknown break-points. Statistics in Medicine, 22(19): 3055-3071. DOI:10.1002/sim.1545

Müller, K. et al., 2004. Investigating the wavelet coherence phase of the BOLD signal. Journal of Magnetic Resonance Imaging: An Official Journal of the International Society for Magnetic Resonance in Medicine, 20(1): 145-152.

Näschen, K., Diekkrüger, B., Leemhuis, C., Seregina, L.S., van der Linden, R., 2019. Impact of Climate Change on Water Resources in the Kilombero Catchment in Tanzania. Water, 11(4): 859.

Ni, S. et al., 2018. Global Terrestrial Water Storage Changes and Connections to ENSO Events. Surveys in Geophysics, 39(1): 1-22. DOI:10.1007/s10712-017-9421-7

Nicholls, N., Lavery, B., Frederiksen, C., Drosdowsky, W., Torok, S., 1996. Recent apparent changes in relationships between the El Niño-Southern Oscillation and Australian rainfall and temperature. Geophysical Research Letters, 23(23): 3357-3360. DOI:10.1029/96GL03166

Pachauri, R.K. et al., 2014. Climate Change 2014: Synthesis Report. Contribution of Working Groups I, II and III to the Fifth Assessment Report of the Intergovernmental Panel on Climate Change. IPCC, Geneva, Switzerland, 151 pp.

Peixoto, J.P., Oort, A.H., 1992. Physics of climate. American Institute of Physics, New York, United States, 271 pp.

Percival, D.B., Walden, A.T., 2000. Wavelet methods for time series analysis, 4. Cambridge university press.

Ramillien, G., Frappart, F., Seoane, L., 2014. Application of the Regional Water Mass Variations from GRACE Satellite Gravimetry to Large-Scale Water Management in Africa. Remote Sensing, 6(8): 7379-7405.

Rayner, N.A. et al., 2003. Global analyses of sea surface temperature, sea ice, and night marine air temperature since the late nineteenth century. Journal of Geophysical Research: Atmospheres, 108(D14): 4407. DOI:10.1029/2002jd002670

Reager, J.T., Famiglietti, J.S., 2009. Global terrestrial water storage capacity and flood potential using GRACE. Geophysical Research Letters, 36(23): L23402. DOI:10.1029/2009GL040826

Rieser, D., Kuhn, M., Pail, R., Anjasmara, I.M., Awange, J., 2010. Relation between GRACE-derived surface mass variations and precipitation over Australia. Australian Journal of Earth Sciences, 57(7): 887-900. DOI:10.1080/08120099.2010.512645

Rodell, M., Beaudoing, H.K., 2017. GLDAS Noah Land Surface Model l4 monthly 1.0× 1.0 degree V2. 1. Goddard Earth Sciences Data and Information Services Center (GES DISC), Greenbelt, MD, USA. DOI:10.5067/LWTYSMP3VM5Z

Running, S., Mu, Q., Zhao, M., 2017. MOD16A2 MODIS/Terra Net Evapotranspiration 8-Day L4 Global 500m SIN Grid V006. NASA EOSDIS Land Processes DAAC, 6. DOI:https://doi.org/10.5067/MODIS/MOD16A2.006

Sakumura, C., Bettadpur, S., Bruinsma, S., 2014. Ensemble prediction and intercomparison analysis of GRACE time - variable gravity field models. Geophysical Research Letters, 41(5): 1389-1397.

Schmidt, R. et al., 2006. GRACE observations of changes in continental water storage. Global and Planetary Change, 50(1-2): 112-126.

Sharma, R.H., Shakya, N.M., 2006. Hydrological changes and its impact on water resources of Bagmati watershed, Nepal. Journal of Hydrology, 327(3-4): 315-322.

Shukla, K.A., Ojha, S.C., Singh, P.R., Pal, L., Fu, D., 2019. Evaluation of TRMM Precipitation Dataset over Himalayan Catchment: The Upper Ganga Basin, India. Water, 11(3): 613. DOI:10.3390/w11030613

Su, X., Ping, J., Ye, Q., 2011. Terrestrial water variations in the North China Plain revealed by the GRACE mission. Science China Earth Sciences, 54(12): 1965-1970.

Sun, Z., Zhu, X., Pan, Y., Zhang, J., 2017. Assessing Terrestrial Water Storage and Flood Potential Using GRACE Data in the Yangtze River Basin, China. Remote Sensing, 9(10): 1011. DOI:10.3390/rs9101011

Swenson, S., Chambers, D., Wahr, J., 2008. Estimating geocenter variations from a combination of GRACE and ocean model output. Journal of Geophysical Research: Solid Earth, 113(B8): B08410. DOI:10.1029/2007JB005338

Swenson, S., Wahr, J., 2006. Post-processing removal of correlated errors in GRACE data. Geophysical Research Letters, 33(8): L08402. DOI:10.1029/2005GL025285

Tang, J., Cheng, H., Liu, L., 2014. Assessing the recent droughts in Southwestern China using satellite gravimetry. Water Resources Research, 50(4): 3030-3038.

Tapley, B.D., Bettadpur, S., Watkins, M., Reigber, C., 2004. The gravity recovery and climate experiment: Mission overview and early results. Geophysical Research Letters, 31(9): L09607. DOI:10.1029/2004gl019920

Torrence, C., Webster, P.J., 1999. Interdecadal changes in the ENSO–monsoon system. Journal of climate, 12(8): 2679-2690.

Vuille, M., Bradley, R.S., Keimig, F., 2000. Climate variability in the Andes of Ecuador and its relation to tropical Pacific and Atlantic sea surface temperature anomalies. Journal of Climate, 13(14): 2520-2535.

Wahr, J., Molenaar, M., Bryan, F., 1998. Time variability of the Earth's gravity field: Hydrological and oceanic effects and their possible detection using GRACE. Journal of Geophysical Research: Solid Earth, 103(B12): 30205-30229.

Wang, B., An, S., 2002. A mechanism for decadal changes of ENSO behavior: Roles of background wind changes. Climate Dynamics, 18(6): 475-486.

Wang, B., Chan, J.C., 2002. How strong ENSO events affect tropical storm activity over the western North Pacific. Journal of Climate, 15(13): 1643-1658.

Wang, B., Li, T., 2004. EAST ASIAN MONSOON-ENSO INTERACTIONS, East Asian Monsoon. World Scientific Series on Asia-Pacific Weather and Climate. WORLD SCIENTIFIC, pp. 177-212. DOI:10.1142/9789812701411_0005

Wang, B., Wu, R., Lau, K., 2001. Interannual variability of the Asian summer monsoon: Contrasts between the Indian and the western North Pacific–East Asian monsoons. Journal of climate, 14(20): 4073-4090.

Wang, H., 2001. The weakening of the Asian monsoon circulation after the end of 1970's. Advances in Atmospheric Sciences, 18(3): 376-386. DOI:10.1007/BF02919316

Wang, H., 2002. The instability of the East Asian summer monsoon–ENSO relations. Advances in Atmospheric Sciences, 19(1): 1-11. DOI:10.1007/s00376-002-0029-5

White, D., Richman, M., Yarnal, B., 1991. Climate regionalization and rotation of principal components. International Journal of Climatology, 11(1): 1-25.

Xie, Y. et al., 2018. GRACE-Based Terrestrial Water Storage in Northwest China: Changes and Causes. Remote Sensing, 10(7): 1163.

Xu, Z., Fan, K., Wang, H., 2015. Decadal variation of summer precipitation over China and associated atmospheric circulation after the late 1990s. Journal of Climate, 28(10): 4086-4106.

Yamamoto, K., Fukuda, Y., Nakaegawa, T., Nishijima, J., 2007. Landwater variation in four major river basins of the Indochina peninsula as revealed by GRACE. Earth, planets and space, 59(4): 193-200.

Yang, F., Lau, K.M., 2004. Trend and variability of China precipitation in spring and summer: linkage to sea‐surface temperatures. International journal of climatology, 24(13): 1625-1644.

Yang, P., Zhan, C., Xia, J., Han, J., Hu, S., 2018. Analysis of the spatiotemporal changes in terrestrial water storage anomaly and impacting factors over the typical mountains in China. International Journal of Remote Sensing, 39(2): 505-524. DOI:10.1080/01431161.2017.1388939

Zhang, C. et al., 2017. Tracing changes in atmospheric moisture supply to the drying Southwest China. Atmospheric Chemistry and Physics, 17(17): 10383-10393. DOI:10.5194/acp-17-10383-2017

Zhang, D., Zhang, Q., Werner, A.D., Liu, X., 2016. GRACE-based hydrological drought evaluation of the Yangtze River Basin, China. Journal of Hydrometeorology, 17(3): 811-828.

Zhang, Z., Chao, B., Chen, J., Wilson, C.R., 2015. Terrestrial water storage anomalies of Yangtze River Basin droughts observed by GRACE and connections with ENSO. Global and Planetary Change, 126: 35-45.

Zhao, Q., Wu, W., Wu, Y., 2015. Variations in China's terrestrial water storage over the past decade using GRACE data. Geodesy and Geodynamics, 6(3): 187-193. DOI:https://doi.org/10.1016/j.geog.2015.03.004

Zhou, T.-J., Yu, R.-C., 2005. Atmospheric water vapor transport associated with typical anomalous summer rainfall patterns in China. Journal of Geophysical Research: Atmospheres, 110(D8): D08104. DOI:10.1029/2004JD005413

Zhu, C., Lee, W.-S., Kang, H., Park, C.-K., 2005. A proper monsoon index for seasonal and interannual variations of the East Asian monsoon. Geophysical Research Letters, 32(2): L02811. DOI:10.1029/2004GL021295

Appendices

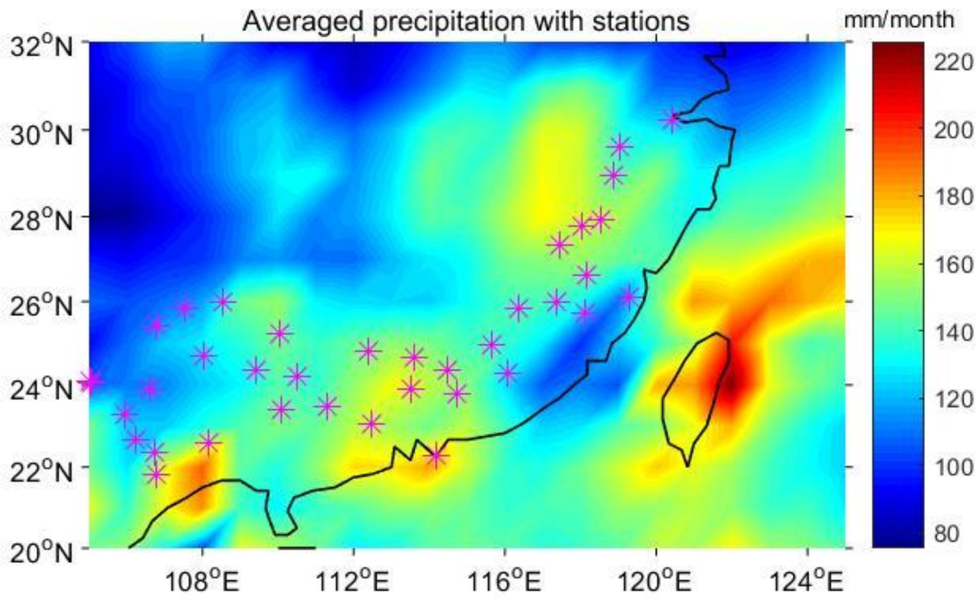

Figure S1. The averaged precipitation during 2003 and 2015 over southeast China. The magenta asterisks (*) are the precipitation stations.

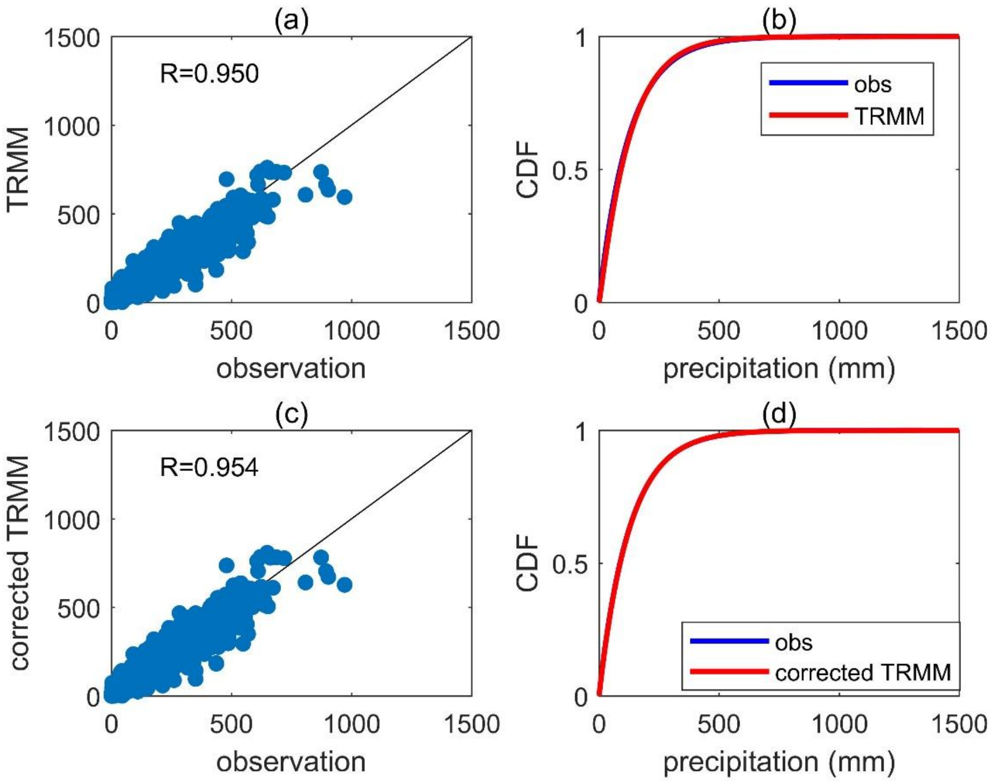

Figure S2. (a) The scatter plot of observed and TRMM precipitation in south China, and (b) comparison of their Gamma CDFs. (c-d) same as (a-b), but for observation and corrected TRMM.

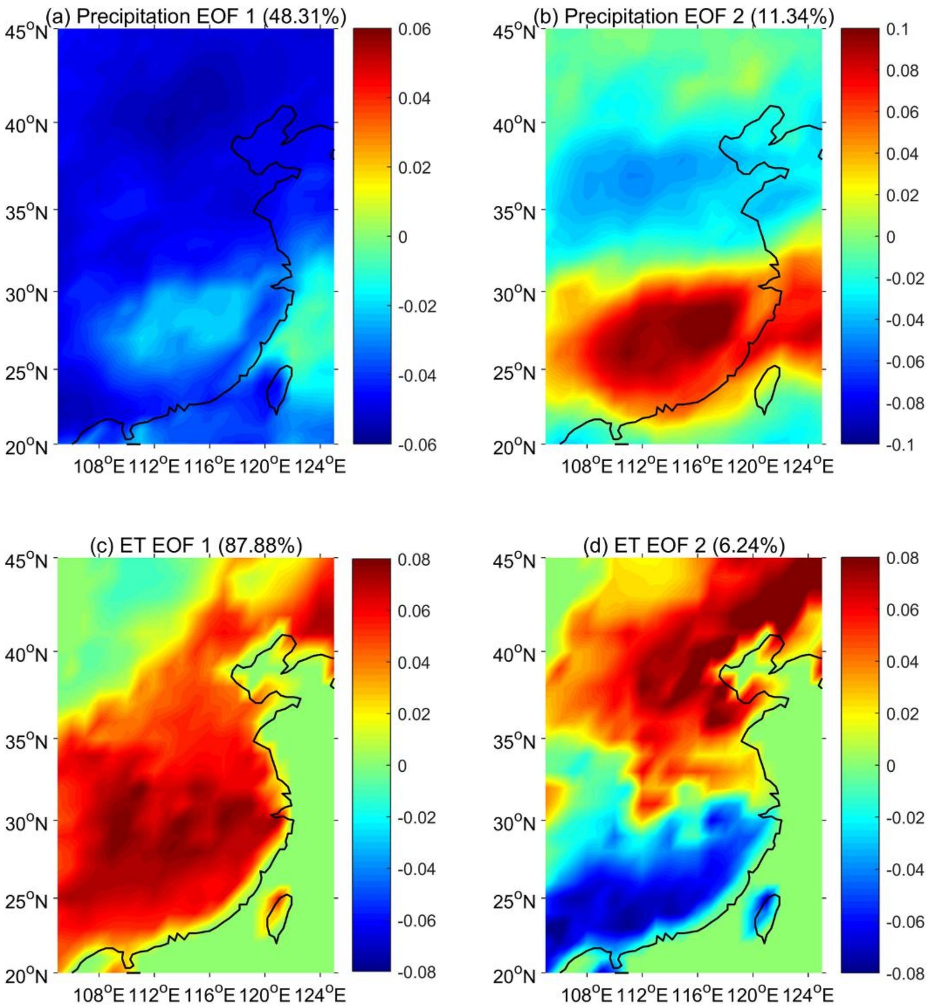

Figure S3. The first and second EOFs of TRMM precipitation (a-b) and ET (c-d).

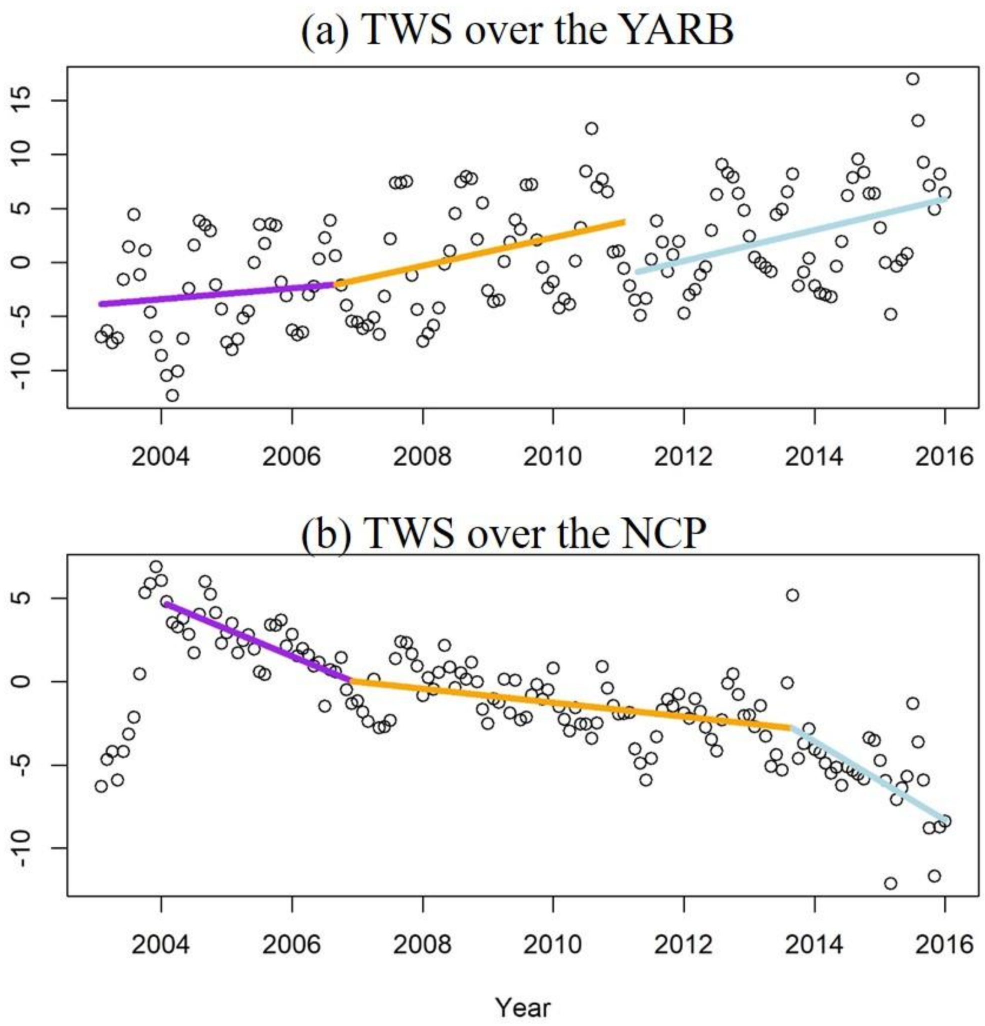

Figure S4. The Break-point analysis for the TWS time series over the YARB (a) and the NCP (b).

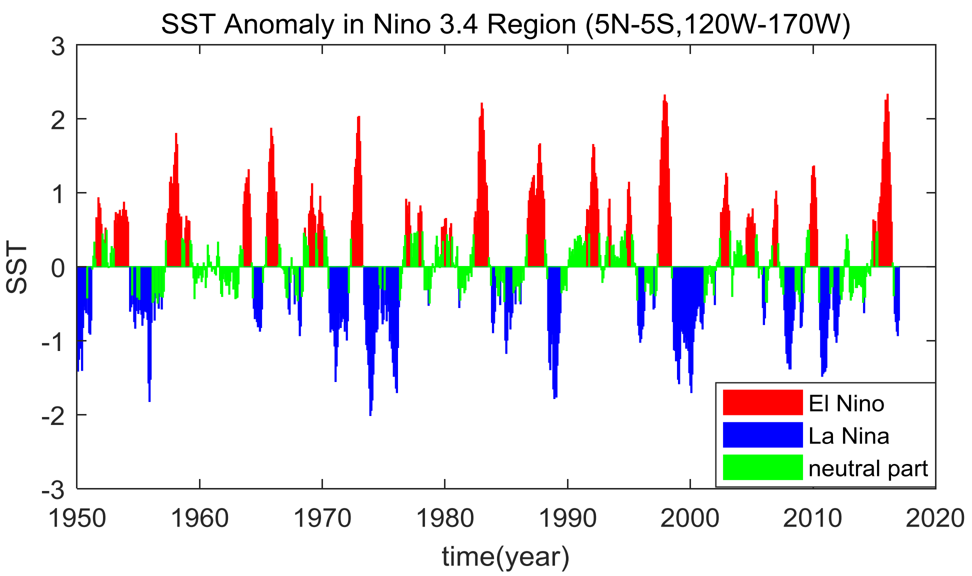

Figure S5. El Nino (red), La Nina (blue) and neutral part (green) from 1950 to 2016.

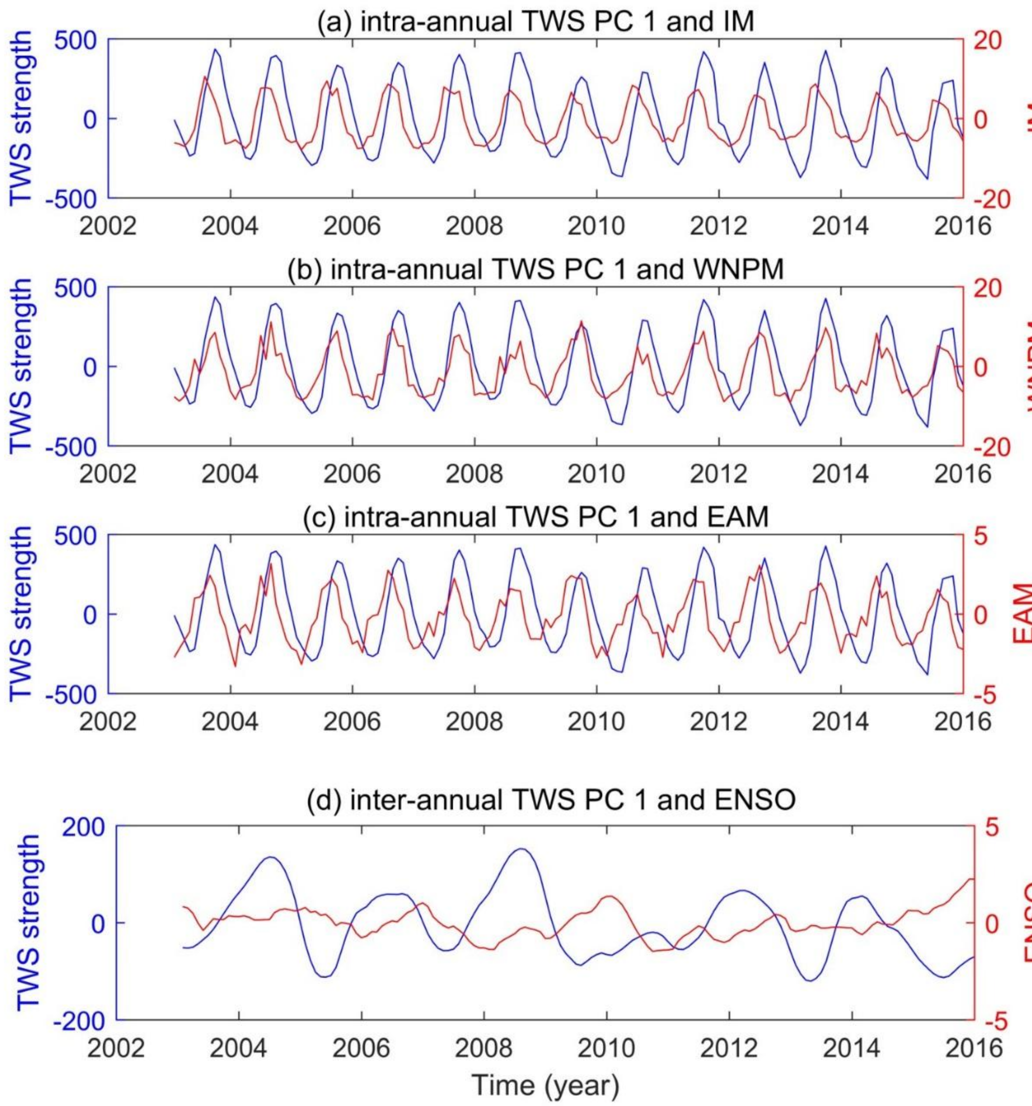

Figure S6. The TWS PC 1 against the Asian monsoons on intra-annual scale (a-c) and ENSO on inter-annual scale (d) with 1-2 and 4 months lag, respectively.